Analysis of a 2-3 exchange symmetric neutrino mass matrix.

Michael Warren McCutcheon, Dept. of Physics, McGill University, Montreal.

August, 2002.

A thesis submitted to the Faculty of Graduate Studies and Research in partial fulfilment of the requirements of the degree of MSc.

National Library of Canada

Acquisitions and Bibliographic Services

395 Wellington Street
Ottawa ON K1A 0N4
Canada

Bibliothèque nationale du Canada

Acquisisitons et services bibliographiques

395, rue Wellington
Ottawa ON K1A 0N4
Canada

Your file Votre référence
ISBN: 0-612-88263-2
Our file Notre référence
ISBN: 0-612-88263-2

Résumé.

Nous présentons une analyse de la nécessité d'une symétrie d'échange 2-3 dans la matrice de masse de neutrino en comparaison avec l'intervalle expérimental admissible pour les paramètres d'oscillations de neutrino. La matrice symétrique, définie à une énergie appropriée pour un neutrino droitier dans le modèle de suppression de masse en dents de scie, subit une évolution suite aux équations supersymétriques du groupe de renormalisation, afin d'interpréter la matrice avec les énergies expérimentales. Nous discuterons du status de la présence de la masse du neutrino dans le modèle standard et justifierons le contexte de cette analyse en examinant les mécanismes et les éléments de preuve d'oscillations. Ensuite, nous parcourrons le mécanisme en dents de scie, ainsi que le processus de renormalisation et son rôle de pont entre les deux échelles d' énergies disparates. Les équations du groupe de renormalisation qui sont applicables seront présentées et la paramétrisation des effets pertinents du groupe de renormalisation sera démontrée. Enfin, nous décriverons des travaux antérieurs sur l'analyse de cette symétrie avant de mettre à jour leurs résultats et d'étendre l'analyse au comportement global dans l'ensemble des paramètres d'oscillations de neutrino à la fois solaire et atmosphérique.

Abstract.

We present an analysis of the requirements of a 2-3 exchange symmetry in the neutrino mass matrix in comparison to the experimentally allowed ranges of neutrino oscillation parameters. The symmetric matrix, being defined at an energy scale appropriate to a right-handed neutrino in a See-saw scheme of mass suppression, is subject to evolution under Supersymmetric Renormalisation Group Equations, in order to interpret the matrix at experimental energies. By way of motivation we discuss the status of neutrino mass in the Standard Model and justify the context of the analysis by examining the mechanisms and evidence for oscillations. We then review the See-saw mechanism and also the process of renormalisation and its implications for bridging disparate energy scales. We present the relevant Renormalization Group Equations and demonstrate the parameterisation of pertinent Renormalization Group effects. Finally, we review previous work analysing this symmetry before updating some of these results and extending the analysis to its global behaviour in the space of both solar and atmospheric neutrino oscillation parameters.

Acknowledgements.

My deepest thanks are due to Prof. C. S. Lam for his patience and advice. Thanks also to my parents, Niall and Carol, for their support. I would also like to extend my appreciation to my friends within the McGill Physics Department for their wit and wisdom, especially Alex Bourque who also helped greatly with the translation of the abstract, and those without for their encouragement. Special thanks to Erica Maraillet for her understanding and enthusiasm. I am indebted to the Department's generosity, including it's policy of waiving the fee differential for International Students, without which this valuable experience would have been impossible. All numerical calculations in this work were performed using MapleV Release 5.0.

Contents

1 Introduction. **1**

1.1 Neutrino mass in the Standard Model. 5

1.2 Neutrino oscillations. 8

1.2.1 Mechanism. 8

1.2.2 Matter effects. 12

1.2.3 Evidence. 15

2 Background. **21**

2.1 The See-saw mechanism. 22

2.2 Renormalisation and running couplings. 24

2.2.1 Regularization. 27

2.2.2 Renormalization. 31

2.2.3 Running couplings and the Renormalization Group. 33

2.3 Supersymmetry. 36

3 Application. **40**

3.1 Renormalisation of See-saw scale symmetries. 41

3.2 Constraints from a simple See-saw scale neutrino symmetry. . 44

3.2.1 Symmetry relations. 44

3.2.2 Global analysis. 47

3.2.3 Space of solar parameters. 54

3.2.4 Space of atmospheric parameters. 56

A Useful Identities for Dimensional Regularization [33]. 73

List of Tables

1.1 Best-fit oscillation parameters. 18

2.1 c_F^k in the SM. 35
2.2 b_k in the SM. 35
2.3 b_k in SUSY. 38
2.4 c_F^k in SUSY. 39

3.1 I_τ and I_μ with $\tan\beta$. 42
3.2 Original oscillation parameters. 46
3.3 Revised values of minimum m_0. 47
3.4 Upper limits on R. 53
3.5 Prefered ranges of m_0. 66

List of Figures

2.1 Tree-level scattering. 24
2.2 Next-to-lowest order scattering in QED. 25
2.3 Observed coupling as a diagram series. 26
2.4 QED scattering to one-loop. 27
2.5 Re-define the observed charge. 31

3.1 Behaviour of the model in LMA. 49
3.2 Behaviour of the model in LOW. 50
3.3 Contours of $(+t_3)^2$ in solar space. 54
3.4 Contours of $(-t_3)^2$ in solar space. 55
3.5 R against t_2^2 under the normal hierarchy. 57
3.6 R against t_2^2 under the inverted hierarchy. 58
3.7 $\log((+t_3)^2)$ against t_2^2 across $t_2^2 = 1$. 59
3.8 $\log((-t_3)^2)$ against t_2^2 across $t_2^2 = 1$. 59
3.9 (LMA, +) contours of $(+t_3)^2$ in atm. space: $m_0 = 0.05$eV. . . 61
3.10 (LMA, $-$) contours of $(-t_3)^2$ in atm. space: $m_0 = 0.05$eV. . . 62
3.11 (LOW, +) contours of R in atm. space: $m_0 = 0.0500$eV. . . . 64
3.12 (LOW, +) contours of R in atm. space: $m_0 = 0.01614$eV. . . . 65
3.13 Asymptotic behaviour of t_3^2 against m_0. 67
3.14 (LMA, $-$) contours of m_0 for $t_3^2 = 0.01$. 68
3.15 (LMA, $-$) contours of R for $t_3^2 = 0.01$. 69
3.16 (LMA, $-$) contours of R for $t_3^2 = 0.026$. 70

Chapter 1

Introduction.

Neutrino mass, its status in the Standard Model of Particle Physics, the related phenomenon of neutrino oscillations and why the latter should be of interest.

"I have done a terrible thing, I have postulated a particle that cannot be detected."

-W. Pauli. [1]

Neutrinos are the most elusive and, consequently, least understood of the fundamental particles. They thus attract intense theoretical speculation in attempts to restrict their properties and hence make predictions that may be put to experiment.

Primary to the puzzle of the neutrino has been the nature of its mass. The particle was first hypothesised by Pauli (1931) in order to rescue the conservation of energy in β-decay, where the energy of the emitted electron was not fixed as would be so in the case of a two-body decay. β-decay was originally thought to follow a two-body scheme, where:

$$\begin{array}{rcccccc} & {}^{N}_{Z}A & \rightarrow & {}^{N}_{Z\pm1}B & + & e^{\mp} \\ \text{Energy conservation:} & E_A & = & E_B & + & E_\beta \\ \text{Momentum conservation:} & \mathbf{0} & = & \mathbf{p} & + & (-\mathbf{p}) \end{array}$$

The parent nucleus A decays into its daughter B with the release of a positron or electron (the β-particle). E_β is restricted to $Q = E_A - E_B$ and the three momenta of the daughter nucleus and β-particle must be equal. There is only one set of values for p and E_β that fulfills these criterea. But the observed electron spectra of these decays showed an energy deficit and shape which Pauli recognised could be the signature of a three-body decay. Knowing that a new charged particle would violate charge conservation in the decays, he christened this particle the 'neutron'. But this moniker was lost to the neutral nucleon we know today and the neutral particle associated with β-decay is now recognised as the neutrino.

As the neutrino was invoked as a near invisible carrier of energy, it was natural to ask, how much of the latter would compose its mass? Pauli originally declared a very cautious upper bound of 1% of the proton mass, but it was soon apparent that it would be much less. Thus β-decay presented the most immediate means of searching for neutrino mass.

The principle behind such experiments is that, if neutrinos have a finite mass, the *maximum* energy of the charged products will fall short of the Q-value (the released energy) of the reaction. That is to say, that in the limit in which the neutrino is created at rest (in the rest frame of the parent neucleus) its only influence upon the charged products is in depriving them of its rest energy. This will manifest itself as a truncated β-particle energy spectrum. The most favourable decay for this measurement is that having the lowest Q-value because this will maximise the shortfall at the end-point of the spectrum, relative to its total range.

Inevitably this measurement also deals with effects from nuclear and atomic physics and so a simplistic (low-Z) parent is prefered, in order to limit uncertainities from these domains. To this end, Tritium decay (${}^3_1\text{H} \rightarrow {}^3_2\text{He}^+ + e^-$), having the least Z parent and the second least Q of all β-decays, is an ideal forum for experiments in directly measuring neutrino mass [2].

Such experiments struggle with the fact that they seek to measure the end-point of the β emission spectrum which, by the very nature of a three-body process, occupies a vanishing region of phase-space. This means that the rate of suitable events is very low. In addition the energy lost to the recoil of the nucleus is unmeasurable. Nevertheless, they have succeeded in placing an upper limit of 2.2eV (95% C.L.) on the electron neutrino mass [3], but have never indicated a finite value.

Neutrino mass can also introduce more exotic effects. As we will discuss below, if the neutrino's mass is of the so-called Majorana type, it confounds our notion of particle and anti-particle allowing a process called 'neutrinoless double β-decay' ($2\beta0\nu$). Here the neutrino produced by β-decay is the same as that which induces β-decay. Thus an individual nucleus can emit two β-particles of the same type, by the internal exchange of a neutrino between two of its comprising nucleons. The rate at which this process can occur is related to the size of the Majorana mass and so measurement of this rate can constrain the mass. The Heidelberg-Moscow experiment attempts just such a measurement and predicts $m_{ee} < 0.34$ (0.26)eV at 90% (68%) C.L., [4]where m_{ee} is the effective Majorana mass of the electron neutrino.

However, in the case of mixing between the neutrinos of the three generations (the nature of which will be covered in more detail later), cancellation between phases originating from the Majorana nature of the masses can mask the true size of the individual masses and suppress the effective mass in relation to them. Thus, this constraint does not necessarily supersede that from Tritium β-decay. Recently there has been slight evidence for a non-zero neutrino mass from the same experiment with the most optimistic case allowing m_{ee} =0.11–0.56eV at 95% C.L. with a best-fit of 0.39eV [5], though some doubt surrounds the validity of this claim. As yet there exists no firm prediction of a non-zero electron neutrino mass and other neutrino masses have an even more uncertain status.

1.1 Neutrino mass in the Standard Model.

Matters were not as grave as Pauli feared. The interactions of the neutrino are indeed heavily suppressed as a consequence of the very great mass of the mediators of the weak force. Unlike electromagnetism, where the force can be transmitted by the exchange of real photons at all energies, the massive vector bosons ($W^{\pm}, Z^0$) exchanged in weak interactions result in an effective four fermion interaction (the Fermi interaction) at low energies. Such an interaction is suppressed by a factor of the reciprocal of the mass of the exchanged particle, here a $W^{\pm}$ or Z^0.

Despite this hinderance, after years of work, Reines and Cowan successfully confirmed the detection of neutrinos in 1956 [6], by virtue of very large scintillation detectors in close proximity to a nuclear reactor as an intense source of neutrinos. Through the 1960's a number of vital experiments were condcuted on a massive scale using intense neutrino beams, in order to record their interactions. These provided the results necessary to construct the exchange picture of the weak interactions, as it is outlined above, and the accompanying gauge theory of electroweak interactions, due to Glashow, Weinberg and Salam. This work culminated, around 1974, in the acceptance by most of the scientific community of the existence of weak neutral current interactions,[1] whose effects are often concealed by coexisting electromagnetic effects, except only in neutrino reactions.

These experiments could shed light on such details as coupling strengths and the different interactions allowed by the charged and neutral currents. However, at such large energies it was quite impossible to discern the effects of the neutrino's mass, if indeed it had any.

In the absence of detail, the question of mass in the neutrino sector of the Standard Model was built on some well motivated assumptions. The neutrino mass was known to be extremely small, quite below anything that might be observable, so it was reasonable to assume it to be exactly zero,

[1] Those due to the exchange of the Z^0, in contrast to the charged current interactions resulting from $W^{\pm}$ exchange.

at least as an approximation. In addition, it was discovered that neutrinos were produced only with left-handed chirality, ν_L:

$$\gamma_5\nu = \gamma_5\nu_L = -\nu_L \tag{1.1}$$

which was later attributed to the $(V-A)$ character of the weak interactions.[2] That is to say, charged current interactions (i.e. those responsible for β-decay) couple only states of 'left-handed' chirality.[3] However, chirality is not conserved. This is because the eigenstates of chirality do not, in general, coincide with those of helicity, which *is* conserved as an extension of angular momentum conservation:

$$[\sigma \cdot \mathbf{p}/p]\psi_\pm = \pm\psi^\pm. \tag{1.2}$$

σ are the Pauli spin matricies. A state of definite helicity is thus a linear combination of chiral states:

$$\psi^\pm = a^\pm\psi_L + b^\pm\psi_R, (a^\pm)^2 + (b^\pm)^2 = 1 \tag{1.3}$$

Only in the massless limit, where helicity and chirality do coincide ($a^- = 1, b^+ = 1$), is the latter conserved. Any mass term would mix the chiralities of a neutrino of definite helicity, generating a right-handed component for any neutrino state. In the case that the right-handed component is that of a neutrino (i.e. ν_R) the mass is the 'traditional' Dirac mass, akin to that of the charged fermions. However, a right-handed neutrino would couple to none of the gauge fields and so would not interact: it would be 'sterile'. Thus, if a neutrino carried a Dirac mass there would be an entirely redundant field in the theory.

We can avoid introducing a right-handed neutrino by invoking a Majorana mass. In this case the right-handed component is that of an anti-neutrino (i.e.

[2]Weak interactions are said to have a (*V*ector)$-$(*A*xial vector) structure after the $\bar{\psi}\gamma^\mu[(1-\gamma^5)/2]W_\mu\psi = \bar{\psi}_L\gamma^\mu W_\mu\psi_L$ term in the weak Lagrangian.

[3]Such states are left-handed particles (χ_L) and their antiparticles which are, in fact, right-handed states ($(\chi_L)^C = (\chi^C)_R$). Here $\psi^C = C\bar{\psi}^T = \hat{C}\psi^*$, where $\hat{C} \propto \gamma^2$ is the particle-antiparticle conjugation matrix, and $C \propto \gamma^2\gamma^0$ is the charge conjugation matrix.

$\nu_R^C = (\nu_L)^C$) This represents a mixing of particle and anti-particle and, in the case of neutrinos, a consequent violation of lepton number conservation. If such a mass was possible for charged fermions it would violate charge conservation, by mixing particles of opposite charge, and thus it is forbidden. While charge conservation is the result of a fundamental gauge symmetry, there is no such 'guarding' symmetry to ensure lepton number conservation. But the latter *is* the result of an 'accidental' symmetry of the Standard Model: an unintentional product of the requirements of gauge symmetry and renormalizability. Thus a Majorana mass for a neutrino is beyond the scope of the Standard Model.

The Standard Model escapes such peculiarities as those outlined above by dictating that all neutrinos have exactly zero mass. Indeed, until recently, a non-zero neutrino mass could have been regarded as surplus to requirements.

The Standard Model is very successful: of the twenty-five electroweak parameters measured at the Z^0 resonance in e^+e^- scattering (Table 10.4 of [7]), all but one are in agreement with the Standard Model to 2σ (95% C.L.). But it cannot be a fundamental theory, because it contains almost twenty parameters which are determined only by experiment: within the SM there are no *predictions* (or explanations) for their specific values. It has become a goal of Theoretical High Energy Physics to try to explain these parameters in terms of a deeper theory with the aim of predicting deviations from the behaviour expected within the Standard Model. The great success of the Standard Model attests to the difficultly of detecting such deviations but one obvious realm of exploration is in assessing the assumptions made in the neutrino sector.

1.2 Neutrino oscillations.

It was first suggested by Bruno Pontecorvo (1957)[8] that neutrinos could oscillate: that after a given type of neutrino is produced it may transform into another before detection. At the time this seemed a curiosity and unlikely to be realised in nature. Indeed, it was not confirmed until 1962 that the neutrinos of the different generations were, in fact, distinguishable [9]. And at that point it seemed likely that lepton generation number[4] conservation would forbid oscillations. But in the past decade the phenomenon has attracted renewed interest for reasons that will be discussed below (see Section 1.2.3).

1.2.1 Mechanism.

Oscillation is due essentially to the differing time evolution of the various mass eigenstates (ν_j) of which a given flavour state (ν_α) may be composed.[5]

$$|\nu_\alpha(t)\rangle \;=\; \sum_j U^*_{\alpha j}|\nu_j(t)\rangle \tag{1.4}$$

Such mixing arises from a mismatch between the basis of flavour states and that which diagonalizes the mass matrix. When the basis is rotated from that of the massive states into that of the flavour states, off-diagonal components appear in the mass matrix.

$$\mathcal{L}_{\text{Mass}} \;=\; (\bar{\nu}_1, \bar{\nu}_2, \bar{\nu}_3)[\text{diag}(m_1, m_2, m_3)] \begin{pmatrix} \nu_1 \\ \nu_2 \\ \nu_3 \end{pmatrix} + h.c. \tag{1.5}$$

$$\;=\; (\bar{\nu}_e, \bar{\nu}_\mu, \bar{\nu}_\tau)\mathbf{V}[\text{diag}(m_1, m_2, m_3)]\mathbf{V}^\dagger \begin{pmatrix} \nu_e \\ \nu_\mu \\ \nu_\tau \end{pmatrix} + h.c. \tag{1.6}$$

[4]Initially L_e and L_μ and later, after the discovery of the third generation, L_τ also.

[5]Here $\alpha = e, \mu, \tau$. In general there can also be any number of sterile neutrinos, their multiplicity not being limited by measurements of the Z width which limits the number of light ($m < 90GeV$) neutrinos to three, without ambiguity. However, here I will discount them because experiment disfavours them, as we shall see below. Accordingly $j = 1, 2, 3$.

If we consider the charged current interactions:

$$\mathcal{L}_{CC} = (\bar{e}, \bar{\mu}, \bar{\tau})\gamma^{\lambda}(1-\gamma^5)\begin{pmatrix} \nu_e \\ \nu_\mu \\ \nu_\tau \end{pmatrix} W_\lambda^- + h.c. \tag{1.7}$$

and assume that no other interactions involving charged leptons reveal lepton sector mixing, we may confine mixing to the neutrinos, as is done for down quarks in the quark sector of the SM:[6]

$$\mathcal{L}_{CC} = (\bar{e}, \bar{\mu}, \bar{\tau})_L\gamma^{\lambda}\mathbf{V}\begin{pmatrix} \nu_1 \\ \nu_2 \\ \nu_3 \end{pmatrix}_L W_\lambda^- + h.c. \tag{1.8}$$

Here, $\mathbf{V} = \mathbf{U}$ the Maki/Nakagawa/Sakata (MNS) matrix [10]: the lepton sector counterpart to the Cabibbo/Kobayashi/Maskawa (CKM) matrix [11] of the quarks, which accounts for flavour violation in the weak interactions.

Oscillations will manifest themselves as a conversion between the neutrino flavours. A flavour eigenstate can be identified with a specific mixture of mass states, and as the mass mixture evolves a neutrino may be described by a changing combination of flavours. The probability of observing a neutrino of flavour β, at time t, after the production of a ν_α, at $t = 0$, is given by:

$$P_{\alpha\beta} = |\langle\nu_\beta|\nu_\alpha(t)\rangle|^2 \tag{1.9}$$

As noted, oscillation occurs due to the time evolution of the mass eigenstates, so it is instructive to re-cast $P_{\alpha\beta}$:

$$P_{\alpha\beta} = \Big|\sum_i\sum_j U_{\beta i}U^*_{\alpha j}\langle\nu_i(0)|\nu_j(t)\rangle\Big|^2 \tag{1.10}$$

$$= \Big|\sum_i\sum_j U_{\beta i}U^*_{\alpha j}\exp -iE_jt\langle\nu_i(0)|\nu_j(0)\rangle\Big|^2 \tag{1.11}$$

Where E_j is the energy of the jth mass eigenstate. Now, with

1. $\langle\nu_i|\nu_j\rangle = \delta_{ij}$,

[6]This amounts to allowing the charged fermion mass and flavour eigenstates to coincide.

2. $\sum_{i=1}^{n} a_i \sum_{j=1}^{n} b_j = \sum_{i=1}^{n} a_i b_i + \sum_{j=1}^{(n-1)} \sum_{k=(j+1)}^{n} [a_j b_k + a_k b_j]$

3. $\mathrm{Re}[z] = (z + z^*)/2$

and discarding the imaginary components of the product of mixing matricies, which are CP violating terms, we have:

$$\begin{aligned} P_{\alpha\beta} &= \sum_i^n U^*_{\beta i} U_{\alpha i} U_{\beta i} U^*_{\alpha i} \\ &\quad +2 \sum_{j=1}^{(n-1)} \sum_{k=(j+1)}^{n} \mathrm{Re}[U^*_{\beta j} U_{\alpha j} e^{i(E_j - E_k)t} U_{\beta k} U^*_{\alpha k}] \qquad (1.12) \\ &= \sum_i^n U^*_{\beta i} U_{\alpha i} U_{\beta i} U^*_{\alpha i} \\ &\quad +2 \sum_{j=1}^{(n-1)} \sum_{k=(j+1)}^{n} \Big[\mathrm{Re}[U^*_{\beta j} U_{\alpha j} U_{\beta k} U^*_{\alpha k}] \times \cos(\Delta_{jk} t)\Big] \qquad (1.13) \\ &= \sum_i^n U^*_{\beta i} U_{\alpha i} U_{\beta i} U^*_{\alpha i} \\ &\quad +2 \sum_{j=1}^{(n-1)} \sum_{k=(j+1)}^{n} \Big[\mathrm{Re}[U^*_{\beta j} U_{\alpha j} U_{\beta k} U^*_{\alpha k}] \left(1 - 2\sin^2(\Delta_{jk} t/2)\right) \Big] \qquad (1.14) \\ &= \Big|\sum_i^n U_{\beta i} U^*_{\alpha i}\Big|^2 \\ &\quad -4 \sum_{j=1}^{(n-1)} \sum_{k=(j+1)}^{n} \Big[\mathrm{Re}[U^*_{\beta j} U_{\alpha j} U_{\beta k} U^*_{\alpha k}] \times \sin^2(\Delta_{jk} t/2)\Big] \qquad (1.15) \end{aligned}$$

The first term simplifies to $\delta_{\alpha\beta}$ and $\Delta_{jk} = E_j - E_k$, which in the relativistic limit[7] yields $\Delta_{jk} \approx (p + m_j^2/2E) - (p + m_k^2/2E) = (m_j^2 - m_k^2)/2E$, where, also, $t = L$ the distance travelled.

Here we see the origin of the term neutrino 'oscillations': the terms that lead to metamorphosis of the neutrino type are sinusoidal, with arguments of the type $(m_j^2 - m_k^2)L/4E$ and amplitude $Re[U^*_{\beta j} U_{\beta k} U_{\alpha j} U^*_{\alpha k}]$.

[7]This is certainly reasonable given the upper bound on neutrino masses from direct searches, in comparison with the energy spectra of typical weak decay processes.

The latter is a product of mixing matrix elements that controls the 'strength' of the oscillation which, in a simple two-neutrino scheme, takes the form:

$$\mathrm{U} = \begin{pmatrix} \cos\theta & \sin\theta \\ -\sin\theta & \cos\theta \end{pmatrix}, \tag{1.16}$$

so that:

$$P_{\alpha\beta} = \delta_{\alpha\beta} - (2\delta_{\alpha\beta} - 1)\sin^2(2\theta)\sin^2(\Delta t/2) \tag{1.17}$$

and we may thus assume $0 \leq \theta \leq \pi/2$ and $\Delta \geq 0$ without loss of generality, for the case of two-neutrino oscillations in a vacuum.

The phase evolution of the probability is somewhat more complex: it depends upon the differences between the squared masses[8] , $(m_j^2 - m_k^2) = \Delta m_{jk}^2$. This may be understood as follows. If a neutrino is produced in a given flavour state which is a linear combination of exactly degenerate mass states (e.g. in the SM where all neutrinos have identically zero mass) the time evolution of those states is identical, and the state remains unaltered. Thus neither mixing nor massive neutrinos are by themselves sufficient for oscillation to occur: it is essential that there be a *difference* among the mass eigenvalues. Consequently, if neutrino oscillations are observed then their must exist at least one massive eigenstate, even if the others have exactly zero eigenvalues. Indeed, oscillations are insensitive to the *absolute* value of the masses involved and hence cannot directly place an upper or lower bound on the mass.

The structure of the harmonic terms in the probability allows us to distinguish between the various scenarios in which oscillations are observed. The scale of the squared mass difference, in relation to the energy of the neutrinos involved and the distance over which they are allowed to evolve before observation, sets the number of cycles that the neutrino state will undergo. Specifically, there are three cases of interest:

- $\Delta m_{jk}^2 \gg 4E/L$: the harmonic term varies very rapidly and generally cannot be distinguished by experiment. Such terms are averaged over $(\langle \sin^2(x) \rangle = 1/2)$.

[8]The nature of the mass, be it Dirac or Majorana, does not affect this result.

- $\Delta m^2_{jk} \sim 4E/L$: this case is very favourable for observation. Variations in L and E on the scale of the experiment will result in observable phase shifts which provide detailed information concerning $(m_j^2 - m_k^2)$.
- $\Delta m^2_{jk} \ll 4E/L$: the phase of the harmonic term is little changed with respect to the initial state and oscillations are not observed.

1.2.2 Matter effects.

The foregoing discussion has related to vacuum effects: those occuring during the free propagation of neutrinos. However, additional effects arise from the presence of matter. As neutrinos travel through atomic matter they may partake in coherent elastic scattering with the protons, neutrons and electrons of which it is comprised. These interactions do not directly change the neutrinos but the nett result is that a potential energy term is introduced into the Lagrangian of the neutrinos which will affect their evolution in matter [12]. Interactions with nucleons (protons and neutrons) are through the neutral current only and so their contribution is identical for each of the three active neutrinos. Electrons will also contribute through the neutral current but in addition they will interact through the charged current exclusively with electron neutrinos. Thus electron neutrinos will experience a potential, V_e, different to that felt by muon or tau neutrinos, V_X, and this leads to differences in their evolution within matter.

Consider a system consisting of two neutrino mass eigenstates, $\nu_{1,2}$ with eigenvalues $m_{1,2}$, which, in vacuum, are each a mixture of the electron neutrino, ν_e, and another active neutrino, ν_X which may itself be a combination of muon and tau neutrinos:

$$\begin{pmatrix} \nu_1 \\ \nu_2 \end{pmatrix} = \begin{pmatrix} \cos\theta & \sin\theta \\ -\sin\theta & \cos\theta \end{pmatrix} \begin{pmatrix} \nu_e \\ \nu_X \end{pmatrix}. \tag{1.18}$$

In the presence of matter the differing reaction potentials for the ν_e and ν_X components will alter the mass eigenvalues and the compositions of the mass eigenstates [12], [13]. This amounts to defining an effective mixing angle, θ_m, and effective masses, $\mu_{1,2}$, in matter:

$$\begin{aligned}\mu^1_{1,2} &= \frac{m_1^2 + m_2^2}{2} + E(V_e + VX) \\ &\mp \frac{1}{2}\sqrt{(\Delta m^2 \cos 2\theta - 2E(V_e - V_X))^2 + (\Delta m^2 \sin 2\theta)^2} \quad (1.19)\end{aligned}$$

where $\Delta m^2 = m_2^2 - m_1^2$, E is the neutrino energy and θ_m satisfies:

$$\tan 2\theta_m = \frac{\Delta m^2 \sin 2\theta}{(\Delta m^2 \cos 2\theta - 2E(V_e - V_X)}. \quad (1.20)$$

As noted above the neutral current components of V_e and V_X are identical, so that their difference is simply the charged current contribution which is proportional to the electron number density, N_e, and the effective coupling of weak interactions at low energy, G_F the Fermi coupling [Wolfenstein; 1978]:

$$V_e - V_X = \sqrt{2} G_F N_e. \quad (1.21)$$

Due to the small size of G_F a very great density of matter is required to introduce observable effects through the reaction potential.

In general the density of matter will vary and thus the effective masses and mixing are essentially instantaneous quantities which will vary in time. Evolution of the mixing angle introduces its own distortion in the system such that the instantaneous mass eigenstates, the states associated with the mass eigenvalues $\mu_{1,2}$, will mix and are no longer the instantaneous energy eigenstates which must be considered in examining the evolution of the system. This mixing is proportional to the rate of change of the effective mixing angle, $\dot{\theta}_m$ and thus for slowly varying θ_m this effect is negligible: the so-called *adiabatic* case when $\dot{\theta}_m \ll \Delta\mu^2/4E$.

A consequence of (1.19) and (1.20) is that, for a given neutrino energy, a condition of least difference between the effective masses coincides with maximal mixing at a *resonant* density, ρ:

$$\rho = \frac{\sqrt{2}\Delta m^2}{4 G_F E} \cos 2\theta \quad (1.22)$$

θ_m varies between the θ at low density and $\frac{\pi}{2} - \theta$ above the resonant density. It changes most rapidly close to the resonant density such that non-adiabatic effects may appear.

The existence of the resonant density has important implications for the evolution of neutrinos as they progress through matter. Consider electron neutrinos created in the core of the Sun and having a vacuum mixing angle $\theta < \pi$. Models of the solar interior suggest an approximately exponential decrease in density away from the centre:

$$N_e(r) = N_e(0)e^{-r/r_0}, \quad r_0 = r_\odot/10.54. \tag{1.23}$$

We may then classify three scenarios:

- $\rho \gg N_e(0)$: matter effects are negligble and solar neutrino oscillations behave as in the case of evolution in a vacuum.

- $\rho \gtrsim N_e(0)$: neutrinos do not experience the resonant conditions but matter effects will be significant. Density does not vary sufficiently quickly to introduce non-adiabatic effects so that at each point the effective mass eigenstates may be treated as the energy eigenstates in the usual way. Evolution proceeds by the same mechanism as in vacuum but with the parameters adjusted by the presence of matter.

- $\rho < N_e(0)$: electron neutrinos will be produced in the solar core with $\theta_m > \pi/4$ such that they consist primarily of the ν_2 eigenstate and vice versa. The neutrinos then pass through the resonant state and their behaviour here depends upon the adiabaticity. In the adiabatic case there is little mixing between the ν_1 and ν_2 states and as the ν_2 state passes through resonance and on to the surface it gains primarily ν_X character because θ_m drops below $\pi/4$. For small θ the transformation of ν_e flux to ν_X is actually enhanced: this is the MSW effect [12], [13]. In the non-adiabatic case the mixing between the instantaneous mass eigenstates in the large $\dot{\theta}_m$ region around resonance weakens the MSW effect: e.g. an energy eigenstate that could be associated with ν_2 in a region of small $\dot{\theta}_m$ above resonance, will acquire some ν_1 character during resonance, increasing the component that will boost ν_e flux at the surface.

It is apparent from the preceding dicussion that matter effects introduce a rich and complex structure into the problem of understanding solar neutrinos.

1.2.3 Evidence.

Interest in neutrino oscillations has been aroused in the last decade by puzzling experimental results. In 1967 the Homestake experiment [14] began to measure the flux of electron neutrinos from nuclear fusion reactions in the core of the Sun. Such an endeavour is by no means trivial and requires a very large detector and a great deal of patience. The results were surprising in that there was an apparent deficit of around two-thirds compared to the flux expected from models of the Sun's structure and the nuclear processes at its centre. For some time this was the only experiment in the field, as the data slowly accumulated in favour of this deficit.

When other experiments sensitive to solar neutrinos began, in the late 1980's and early 1990's, it became apparent that this was genuinely due to a neutrino deficit and not an artifact of the experiment. Though there was some variation between experiments in the observed flux, ranging from ~ 0.3 to ~ 0.6 of that which was expected, the shortfall was beyond doubt. In light of the success of the SM, these results called into question our understanding of the solar interior and the various fields within physics which overlap in this domain as embodied in the Solar Standard Model (SSM) [15]. However, recent results from helioseismology [16] support predictions of the SSM suggesting that the origin of the neutrino deficit lies in assumptions within the SM.

Experiments.

Existing experiments fall into two categories: radiochemical and water Čerenkov.

The first relies on the transmutation of nuclei in a bulk sample into radioactive species, by the absorbtion of neutrinos above the energy threshold of the reaction. For instance Homestake [17] uses a large tank containing some 615 tonnes of C_2Cl_4, of which the ^{37}Cl component (approximately 3.6×10^6mol) may be transformed into ^{37}Ar, an unstable isotope with a half-life of 34.8 days. The Argon so produced, being a noble gas, can easily be separated from the bulk fluid and its quantity determined by the event rate measured in the gases extracted. Similar in concept are the Gallium detectors, the first of which was SAGE [18] , starting in 1990, closely follwed by GALLEX [19] in 1991, the latter bieng replaced in 1998 by GNO [20]. They use ^{71}Ga, as either a liquid metal or as a salt in solution, which may be converted into radioactive ^{71}Ge. The principle advantage of all of the above detectors is their great sensitivity, especially the Gallium experiments which have the lowest energy threshold of all. However, all of these experiments can only measure the total flux of electron neutrinos: they are blind to the trajectory of the incident neutrinos and are unable to detect those which are not of the electron type. The latter is critical, because neutrino oscillations will preserve the overall flux of neutrinos but change the proportions of flavours which comprise it.

For these properties we must turn to the second type of experiment. The forebear of this field was Kamiokande [21] which did not begin its life, in 1987, as a neutrino experiment, but rather as a nucleon decay experiment, testing the limits of Grand Unified Theories such as Supersymmetry, which will be discussed later. In fact, in the original conception of the detector, neutrinos were a source of unwanted background noise. As interest in the solar neutrino problem grew, the experiment changed its emphasis to neutrino detection and was upgraded to SuperKamiokande (SK) between 1995 and 1996 [22].

These experiments detect the recoiling charged leptons (electrons or muons)[9] produced by the interaction of neutrinos with the bulk matter of the Earth or the detector. This is achieved by the use of photo-multipliers to detect the faint Čerenkov flash emitted as the recoiling lepton passes through the detector volume. This method has the advantage of being able to resolve events as they happen and also to reconstruct the direction of the lepton from the pattern of light detected. However, to generate the Čerenkov glow a given

[9] Tau particles decay too rapidly to be observed directly.

lepton must exceed the effective speed of light for the medium through which it is travelling. Thus only the most energetic neutrinos will be able to trigger events in these detectors but the more energetic the event the more light will be emitted as Čerenkov radiation and this provides the technique with some energy resolution.

SuperKamiokande relies on the detection of charged leptons which may be attributed to inelastic neutrino scattering, but these must be charged current events which precludes the measurement of τ neutrino flux. The Sudbury Neutrino Observatory (SNO) which began operation in late 1999 [23] will account for this weakness by using heavy water (D_2O) as the core of a spherical Čerenkov detector. The neutron in each deutirium nucleus will be sensitive to neutral current interactions which, for sufficiently energetic neutrinos, will lead to the disintegration of the nucleus. Such events may then be detected from the eventual decay or capture of the resulting free neutron. Crucially, this sensitivity to the neutral current will provide a perfectly balanced measure of the entire flux of active neutrinos, which all experience an identical neutral current interaction. This is the first measure of the total flux and will prove wether or not neutrinos are changing character or are simply under-produced [24].

The energy sensitivity of water Čerenkov experiments has revealed an energy dependence in the neutrino fluxes [22]. In addition directional information has shown a zenith angle dependence in the flux of atmospheric neutrinos [25], which translates into a dependence upon the distance from the production site in the upper atmosphere. Thus the varying detection rates must be explained by an energy and distance dependent phenomenon which supresses the expected yield of events for a given neutrino type. Neutrino oscillations are just such a phenomenon.

Results.

Following [26], a first approximation in examining the experimental evidence for neutrino oscillations is to assume a simple process of oscillation between only two neutrino types. Such an approximation suggests a small squared mass difference drives the solar neutrino oscillation ($10^{-7} - 10^{-5}\text{eV}^2$) and a much larger one the atmospheric oscillation (10^{-3}eV^2). Both scenarios also favour large mixing angles, which is to say that the original flavour state in each contains a significant component of the two mass eigenstates involved, though experiment excludes maximal mixing for solar oscillations ($\tan\theta_{\odot} \neq 1$). Specifically, there are a number of separate regions in the space of solar oscillation parameters any of which could account for the solar neutrino problem. This diversity arises from the myriad scenarios involving matter effects which will affect the evolution of electron neutrinos generated at the Sun's core. Of the various possible scenarios we will consider only the two most likely: LMA and LOW. Experiment defines a single region in the atmospheric neutrino parameter space, where matter effects have little significance and oscillations proceed as in vacuum. The most recent best-fit values for atmospheric [26] and solar [24] neutrino oscillations are shown in Table 1.1.

Scenario	Atm.	LMA	LOW
$\Delta m^2/\text{eV}^2$	2.6×10^{-3}	5.0×10^{-5}	7.9×10^{-8}
$\tan^2\theta$	1.42	0.42	0.61

Table 1.1: Best-fit oscillation parameters.

In addition, the assumption that either solar or atmospheric neutrinos oscillate with a sterile neutrino species is disfavoured.

The preceding analysis turns out to be largely correct. Of course three active neutrinos are known to exist and the mixing scheme should incorporate this. For these purposes the MNS matrix is parameterized as follows:

$$U = \begin{pmatrix} c_{12}c_{13} & s_{12}c_{13} & s_{13}e^{-i\delta} \\ -s_{12}c_{23} - c_{12}s_{23}s_{13}e^{i\delta} & c_{12}c_{23} - s_{12}s_{23}s_{13}e^{i\delta} & s_{23}c_{13} \\ s_{12}s_{23} - c_{12}c_{23}s_{13}e^{i\delta} & c_{12}s_{23} - s_{12}c_{23}s_{13}e^{i\delta} & c_{23}c_{13} \end{pmatrix} \tag{1.24}$$

Where: $s_{ij}(c_{ij}) = \sin\theta_{ij}(\cos\theta_{ij})$ It is conventional in the three neutrino context to take θ_{12} as the mixing angle for solar neutrinos and θ_{23} that for atmospheric neutrinos. Generally, $0 < \theta_{ij} < \pi/2$ and so, in order to cover the whole range, experimental analyses will express mixing in terms of $\tan\theta_{ij} = t_{ij}$, as in Table 1.1. The Dirac phase, δ, may be set to zero or π to preclude CP violating effects due to imaginary components. Both Majorana phases have been set to zero as they cannot influence oscillations [27].

As implied previously, harmonic terms in the conversion probability with disparate mass differences are not influential simultaneously but will come into play individually, under different circumstances depending upon the magnitude of E/L. Thus in constructing a universal picture of oscillations it can be assumed that the solar and atmospheric scenarios are largely unrelated because they occur at quite different scales: in experiments sensitive to solar neutrino oscillations the atmospheric type oscillation is averaged over and in atmospheric experiments the solar type oscillation is negligible.

The two schemes are however related by one parameter, namely θ_{13}, which results in slight deviations from the decoupled, two neutrino, schemes for the solar and atmospheric oscillations mentioned above. In this context, the CHOOZ experiment [28], which aimed to register the disappearance of electron neutrinos originating from a nuclear power plant, places an upper bound on θ_{13} of $\sim 9°$ (90% C.L.), assuming large Δm^2_{13}. The latter assumption is quite reasonable here when we consider the condition: $\Delta m^2_{32} + \Delta m^2_{21} = \Delta m^2_{31} \approx \Delta m^2_{32}$. All the currently available data for solar and atmospheric oscillations favour small values of θ_{13} and the CHOOZ experiment reinforces this trend. Thus, the large mixing of both solar and atmospheric neutrinos is preserved in the three-neutrino mixing scheme.

One artifact of this mixing scheme is that the fit to data is satisfied equally well for two mass hierarchies. The first is the normal hierarchy, analogous to the charged lepton sector or the quarks where: $m_1 < m_2 < m_3$. But an *inverted* hierarchy is also admitted, where: $m_3 < m_1 < m_2$ and $|\Delta m^2_{atm}| = -\Delta m^2_{32} > 0$. The condition of $m_1 < m_2$ is common to both hierarchies and this is due to the fact that the prefered regions in the solar parameter space are possible because of the MSW effect, which requires that the electron neutrino be lighter than the muon neutrino.

Neutrino oscillations describe well the missing solar and atmospheric neutrinos and this constitutes the first evidence of massive neutrinos and hence physics beyond the SM. Such New Physics should explain various peculiar characteristics, such as the near vanishing mass (in relation to other masses in the SM) of the neutrinos, but also the structure of their mass spectrum and the pattern of mixing: the so-called 'texture' of the flavour mixing matrix. It is our task to assess the predictions of a possible texture as it is understood in the background of a likely scheme of New Physics.

The following chapter will outline some of the New Physics, namely the See-Saw Mechanism and Supersymmetry, in addition to techniques necessary for translating this scheme into the realm where experiments are made, namely Renormalisation. The final chapter will deal with their application to the problem at hand: the analysis of a so-called 2-3 exchange symmetry of the neutrino mass matrix, due to C.S. Lam [29].

Chapter 2

Background.

The See-saw mechanism indicates that neutrino physics could probe very high energies, renormalisation allows the extrapolation of predictions from such scales and supersymmetry provides a possible window to the dynamics there.

2.1 The See-saw mechanism.

The masses of the neutrinos are puzzling by their minuteness in relation to other masses in the SM. Specifically, the inclusion of a neutrino with a finite, but very small, mass into a given generation will extend the mass spectrum of that generation over many more orders of magnitude. For the first generation, consisting of the electron and the u and d quarks, the mass ranges from 0.5MeV to ~9MeV: a little more than one order of magnitude. When the electron neutrino is introduced, with a mass certainly less than ~2eV, the mass spectrum must cover at least six orders of magnitude.

Now, the mass scale of the first generation is already very small in comparison to the origin of fermion masses in the SM, namely the Higgs boson Vacuum Expectation Value, v ~100GeV ([30], also Section 2.2.3). But to explain simultaneously the smallness of the first generation masses and, in addition, the extreme smallness of the electron neutrino mass in a simple manner is not trivial.

The See-saw mechanism [31] proposes that the Dirac mass (d) of the neutrino is intrinsically of a similar scale to that of the SM, but that the observed mass (that of the mass eigenstates) is suppressed by a very large Majorana mass, M, of the right-handed neutrino. The Dirac states of the neutrino, ν_d, couple through a mass matrix, $\mathbf{M}$:

$$\begin{aligned} \bar{\nu}_d \mathbf{M} \nu_d &= \begin{pmatrix} \bar{\nu_L} & \bar{\nu_R} \end{pmatrix} \begin{pmatrix} 0 & d \\ d & M \end{pmatrix} \begin{pmatrix} \nu_L \\ \nu_R \end{pmatrix} && (2.1) \\ &= \bar{\nu}_m \mathbf{D} \nu_m && (2.2) \end{aligned}$$

Where ν_m are the mass eigenstates so that $\mathbf{D}$ is diagonal with eigenvalues $\sim \frac{d^2}{M}$ and $\sim M$. The admixture of chiralities for eigenstates in the mass diagonal basis is $\sim \frac{d}{M}$, so that the light neutrino state is predominantly left-handed and thus the mass is predominantly of Majorana character, as might be expected. It is especially interesting that the lightest neutrinos, those that will be observed, have acquired masses even though the left-handed neutrinos, those of the SM, have none.

This simple scenario allows us to make a prediction for the Majorana mass of the right-handed neutrino. For $d \sim$100GeV and $m_\nu(obs.) \lesssim$1eV we can expect $M \gtrsim 10^{13}$GeV. This is a remarkable result and strongly suggests that neutrino physics may be an excellent probe of the physics that exists at energies far beyond those directly accessible to modern experiments.

This scheme may be extended to include multiple generations [32], where the components of $\mathbb{M}$ in (2.2) are matricies themselves. The components representing the right-handed neutrino masses may or may not be identical, but it is simplest to assume that they are similar. Furthermore, it is reasonable to assume that if the mixing matrix between the generations exhibits some degree of symmetry below this scale, then this symmetry will itself be generated at this scale. That is to say that at the scale at which the light neutrino masses are defined, the texture of the mixing matrix generated along side them will be defined by a specific texture. It is attractive to consider that the texture so defined will obey a symmetry indicative of a more fundamental relationship between the generations. But this symmetry may not be immediately apparent at lower energies because the behaviour of neutrinos will actually be different between the vastly disparate energies of, on the one hand, where the fundamental theory is defined and, on the other, where the experiments are carried out.

2.2 Renormalisation and running couplings.

All experimentally observable parameters are determined by the careful measurement of quantum mechanical processes. These processes are described by perturbation theory, in that, to a first approximation, a quantum field theory involves only free fields and interactions are a perturbation to this. This is represented in the structure of the theory by defining a coupling constant $g \ll 1$ which characterises the intrinsic strength of the perturbation. The perturbation expansion on g provides many possible structures, of increasing complexity, for any given interaction. The lowest order form is said to be tree-level from its simple branch- like structure in its representation as a Feynman diagram, where each vertex represents a factor of g.

For example, consider an experiment to measure the coupling of two currents, i.e. the intrinsic likelihood with which they will interfere with one another. The two currents may be arranged so as to pass into close proximity under approximately free motion. Any scattering will be due to their interaction. The lowest order process of this form in Quantum Electro-Dynamics (QED) may be depicted by Fig.2.1, where a fermion current (vector) and an external current (X) interfere by the exchange of a virtual photon (wave).

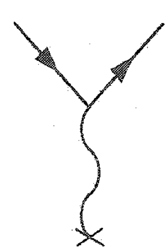

Figure 2.1: Scattering in QED at tree-level: exchange of a single photon with an external current.

The Feynman rules allow us to relate the diagram to an expression for the Lorentz invariant amplitude of the process it represents, from which the probability of the process may be determined. For the above example the rules give:

$$-i\mathcal{M} = ig^2(\bar{u}\gamma^\mu u)(\frac{-ig_{\mu\nu}}{q^2})(j^\nu/g), \tag{2.3}$$

where the term in the first set of parenthesis is the current under observation, the last term in parenthesis is an external current which causes the scattering and g is the coupling we wish to measure. The external current implicitly carries a factor of g from the coupling to the virtual photon. The middle term is associated with the internal photon propagator and depends upon the momentum exchanged between the currents, q.

Higher orders will have more verticies but an identical set of external lines, and hence a more complex internal structure:

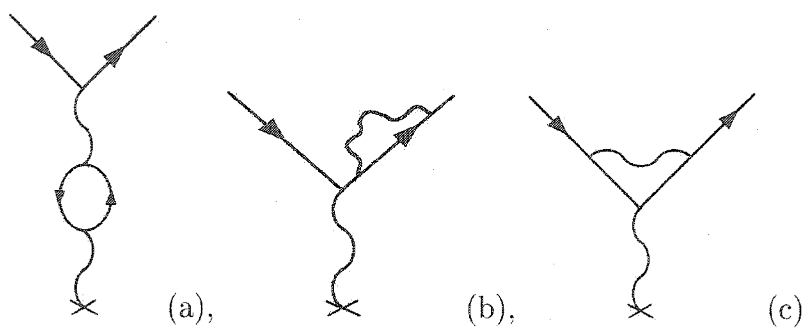

Figure 2.2: QED scattering diagrams at the next-to-lowest order: (a) vacuum polarisation, (b) fermion self-energy and (c) vertex correction.

Each possible structure is indistinguishable to experiments, which can measure only the approximately free, real particles represented by external lines. Thus, in the observation of a given process the experimental measurement encompasses all possible forms of the interaction (see Fig. 2.3).

In order to faithfully represent a given process, as it is observed, we must include all possible diagrams. However, it is convenient to describe the process as a tree-level diagram and we might assume that it is a simple matter to include the contribution of higher-orders by re-defining some property at the tree-level, for instance the coupling in Fig. 2.3. Consequently the observed coupling, g, will not correspond directly to that in the Lagrangian of the theory. Rather the Lagrangian will contain a *bare* coupling, g_0 which

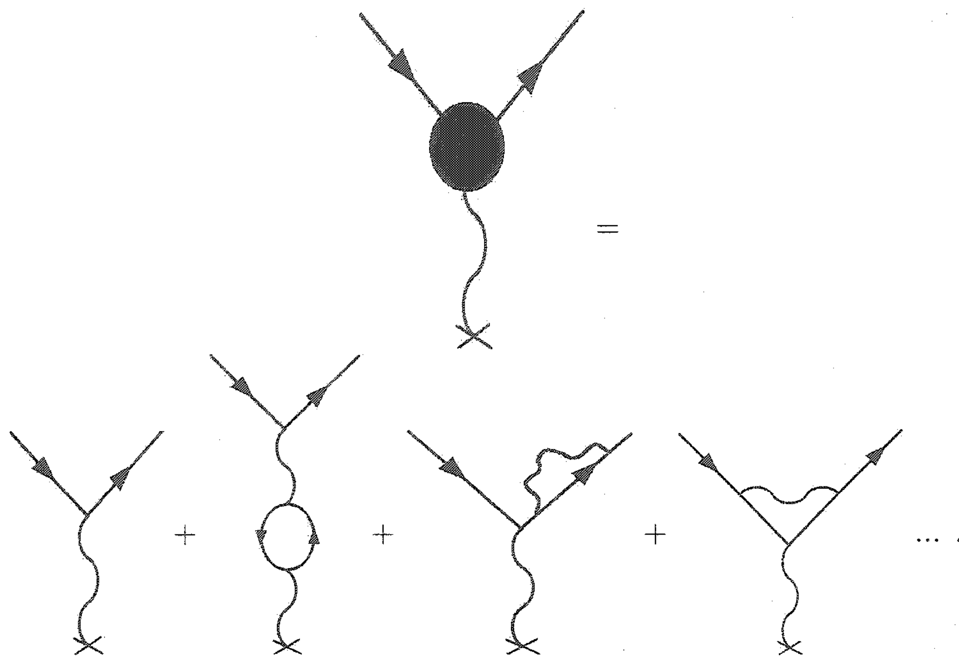

Figure 2.3: The observed coupling is a sum over all possible scattering processes.

is not 'dressed' by higher-order effects. Furthermore, as we are working in perturbation theory so we need include only a few higher-order terms to successfully relate g and g_0.

In fact this approach is by no means trivial. The simplest higher-order diagrams containing even one loop only, result in infinite contributions to g. In principle this is not catastrophic as individual contributions are inherently unobservable. However, to yield a finite value of g the infinite contributions would have to cancel with a quite implausible delicacy, to all orders of the perturbation expansion. To escape this difficulty, the infinite terms may be concealed by a careful re-definition of the bare coupling in a process known as *renormalization*. Firstly we will look at how these infinities may be contained by *regularization* and then we will examine the consequences for observables of this indeterminacy of the theory. This discussion will be restricted to the one-loop level.

2.2.1 Regularization.

When evaluating a diagram, Feynman rules require the integration over the full range of each internal momentum. The rules also require for each vertex a factor of a Dirac delta-function, enforcing momentum conservation at that vertex. At tree-level these rules are sufficient to define all momenta in the diagram and leave a single delta-function which embodies momentum conservation among the external lines. However, at the one-loop level one of the internal momenta remains undefined after all of the delta functions have been taken into account. Thus in the final evaluation of the diagram there remains an integral over an infinite range of momenta. The latter is the origin of the infinite contributions to the observed coupling indicated above.

Looking again at coupling in QED scattering processes to one-loop, we consider:

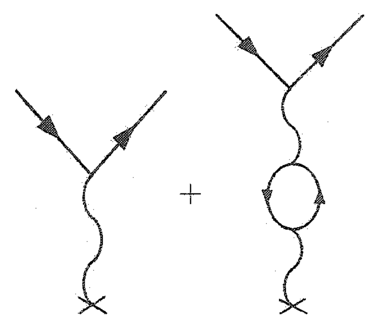

Figure 2.4: Scattering in QED to one-loop.

The one-loop contribution here is solely due to vacuum polarisation as the fermion self-energy and vertex correction cancel exactly by the so-called Ward Identity (p.197 [33]).

The Feynman rules yield:

$$-i\mathcal{M} \quad = \quad ig_0^2(\bar{u}\gamma^\mu u)\Big[\frac{-ig_{\mu\nu}}{q^2} + \frac{-ig_{\mu\alpha}}{q^2}I^{\alpha\beta}\frac{-ig_{\beta\nu}}{q^2}\Big](j^\nu/g_0), \qquad (2.4)$$

The second term inside the square brackets is the *dressed* propagator and carries the contribution of vacuum polarization to the process. $I^{\alpha\beta}$ records the effects of the loop:[1]

$$I^{\alpha\beta} = (-1)^l \int_\forall \frac{\mathrm{d}^4p}{(2\pi)^4} \mathrm{Tr}\left[ig_0\gamma^\alpha \frac{i(\not{p}+m)}{p^2-m^2} ig_0\gamma^\beta \frac{i(\not{p}-\not{q}+m)}{(p-q)^2-m^2}\right] \quad (2.5)$$

$$= -g_0^2 \int_\forall \frac{\mathrm{d}^4p}{(2\pi)^4} \left\{\frac{\mathrm{Tr}[\gamma^\alpha(\not{p}+m)\gamma^\beta(\not{p}-\not{q}+m)]}{[p^2-m^2][(p-q)^2-m^2]}\right\} \quad (2.6)$$

Each loop introduces a factor of -1, so here l=1. The trace derives from the loop structure and the fact that the matrix indicies contract at each of the verticies; the space-time indicies are free and must contract with the photon propagators.

After the angular integral, (2.6) has the form $\int |p|^3 \mathrm{p}/|p|^2$, which will diverge as indicated previously.

A simple means of combatting this anomaly is to restrict the integral to a finite range of momenta by imposing a cut-off. The integral is thereby *regularized*, in that it is no longer divergent. This form of the diagram may now be manipulated in the usual way in calculating scattering cross-sections and the like. Of course the cut-off is an artificial and arbitrary constraint in the theory and in order to cast the final result into the correct form the cut-off must be sent to infinity.

This is certainly a crude and direct means of containing the divergence but it does have an equally straightforward interpretation. It may be seen as indicating that the theory is well defined only at low energies, where the momentum of internal lines is small because the the exchanged momentum must be small. This implies that the anomalous behaviour is linked to our ignorance of more fundamental physics at higher energies and shorter distance scales.

Though this scheme of regularization lends valuable insight, it is flawed. By the uncertainty principle an upper limit on momentum implies a lower limit on position, which effectively discretizes space-time and so violates translational invariance: a fundamental symmetry. Furthermore there is also violation of local gauge symmetries which are a cornerstone of all successful

[1]For clarity the $i\epsilon$ prescription, where $\frac{i(\not{p}+m)}{p^2-m^2} \rightarrow \frac{i(\not{p}+m)}{p^2-m^2+i\epsilon}$ in order to avoid fermion propagator poles, is left implicit.

theories of particle physics.

Fortunately other, more subtle, schemes of regularization have also been developed. One of those that automatically respects local gauge symmetries is *dimensional regularization*, which avoids singularities by the expedient of changing the space-time dimensionality of the problem.

Consider:

$$\int \frac{\mathrm{d}^D k}{(k^2+s)^n} = i\pi^{D/2} \frac{\Gamma(n-D/2)}{\Gamma(n)} \frac{1}{s^{n-D/2}} \tag{2.7}$$

All loop integrals can be reduced to the form of the LHS, with $D = 4$, by Feynaman parameterisation. This procedure reduces the product of quadratic terms in the denominator of an expression, due to propagators in the loop (as in 2.6), to a sum of terms, following the rule:

$$\begin{aligned} \frac{1}{a_0 a_1 \ldots a_n} &= \Gamma(n+1) \int_0^1 \mathrm{d}z_1 \int_0^{z_1} \mathrm{d}z_2 \ldots \int_0^{z_{n-1}} \mathrm{d}z_n \\ &\times \frac{1}{[a_0 + (a_1 - a_0)z_1 + \ldots + (a_n - a_{n-1})z_n]^{n+1}} \end{aligned} \tag{2.8}$$

This form allows use of the standard integrals in Appendix A.

Then we may generalise to $D = 4 - \eta$ and the loop integral will be well defined by the RHS for integer $n > D/2$ or for any non-integer n, specifically small η. Of course all terms within the integral now exist in a space for which $D \neq 4$. This includes the Dirac matricies whose interpretation in non-integer dimensions is by no means clear, but all results are eventually interpreted in the $\eta \to 0$ limit, in which case all relations are reduced to the familiar four-dimensional form. The general D trace and contraction theorems are summarised in Appendix A.

Continuing with the example of QED scattering, we may re-cast (2.6) for general D:

$$I^{\alpha\beta} = -g_0^2 \int_{\forall} \frac{\mathrm{d}^D p}{(2\pi)^4} \left\{ \frac{\mathrm{Tr}[\gamma^\alpha (\not{p} + m)\gamma^\beta (\not{p} - \not{q} + m)]}{[p^2 - m^2][(p-q)^2 - m^2]} \right\} \tag{2.9}$$

Using the trace theorems on the numerator and Feynman parameterisation on the denominator yields:

$$I^{\alpha\beta} =$$
$$-g_0^2 \int_0^1 \mathrm{d}z \int_\forall \frac{\mathrm{d}^D p}{(2\pi)^4} \left\{ \frac{f(D)[(p^\alpha - q^\alpha)p^\beta + (p^\beta - q^\beta)p^\alpha + [m^2 - p(p-q)]g^{\alpha\beta}]}{[p^2 - m^2 + (q^2 - 2pq)z]^2} \right\} \tag{2.10}$$

We can make the substitution $p = k + qz$:

$$\begin{aligned} I^{\alpha\beta} &= -g_0^2 \int_0^1 \mathrm{d}z \int_\forall \mathrm{d}^D k \frac{f(D)}{(2\pi)^4} \Big\{ [2k^\alpha) k^\beta - k^2 g^{\alpha\beta}] + [(q^2 z(z-1) + m^2) g^{\alpha\beta}] \\ &\quad + 2z(z-1)(q^\alpha q^\beta - q^2 g^{\alpha\beta}) \Big\} \times \frac{1}{[k^2 - q^2 z(z-1) - m^2]^2} \end{aligned} \tag{2.11}$$

Here all terms in the numerator linear in k have been dropped as they will be zero by

Using the standard integrals we see that the two terms in square brackets are equal and opposite and thus we are left with:

$$\begin{aligned} I^{\alpha\beta} &= g_0^2 \int_0^1 \mathrm{d}z \frac{f(D)}{(2\pi)^4} \Big[2z(1-z)(q^\alpha q^\beta - q^2 g^{\alpha\beta}) \Big] \\ &\quad \times \frac{i\pi^{D/2}\Gamma(2 - D/2)}{[q^2 z(1-z) - m^2]^{2-D/2}} & (2.12) \\ &= i(q^\alpha q^\beta - q^2 g^{\alpha\beta}) I & (2.13) \end{aligned}$$

Now we examine the case of $D = 4 - \eta$. Using:

$$\Gamma(\frac{\eta}{2}) = \frac{2}{\eta} - \gamma + O(\eta), \tag{2.14}$$

and:

$$s^{-\eta/2} = \frac{\eta}{2} \ln s + O(\eta^2), \tag{2.15}$$

we find that in the limit of $\eta \rightarrow 0$ where regulation is removed:

$$I(q^2) = g_0^2 \Big[\frac{1}{12\pi^2} (\frac{2}{\eta} - \gamma) - \frac{1}{2\pi^2} \int_0^1 \mathrm{d}z z(1-z) \ln(q^2 z(1-z) - m^2) \Big]. \tag{2.16}$$

We see clearly that there is a finite contribution to scattering from vacuum polarisation as well as the troublesome divergence.

2.2.2 Renormalization.

We would like to encapsulate the contribution to scattering of the vacuum polarisation diagram by redefining the charge at the tree-level, as indicated in Fig. 2.5.

With this in mind, from (2.3) and (2.4), we may define:

$$
\begin{aligned}
g^2(g_{\mu\nu}) &\approx g_0^2\left[g_{\mu\nu} + g_{\mu\alpha}I^{\alpha\beta}\frac{-ig_{\beta\nu}}{q^2}\right] && (2.17)\\
&\approx g_0^2\left[g_{\mu\nu} + I_{\mu\nu}\frac{-i}{q^2}\right] && (2.18)\\
&\approx g_0^2(g_{\mu\nu})[1 - I(q^2)] && (2.19)
\end{aligned}
$$

In the final step we have omitted terms in $I_{\mu\nu}$ that are linear in $q_{\mu,\nu}$ as current conservation forbids them from contributing to interactions. In order to define the empirical coupling g without reference to the bare coupling g_0, which introduces the divergent terms, we must rearrange (2.19) to find g_0 in

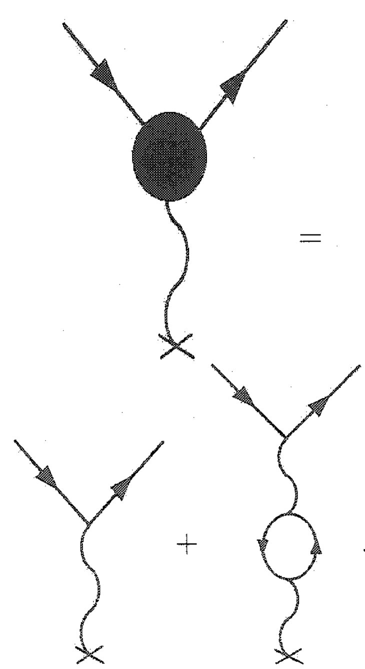

Figure 2.5: We absorb vacuum polarisation into the definition of the observed charge.

terms of g. However (2.19) explicitly depends upon q^2 and so the expression must be evaluated at a specific value of $q = \mu$ in order to define precisely g_0. Thus:

$$g_0^2 \approx g^2(\mu)[1 - I(\mu^2)]^{-1} \tag{2.20}$$

Note that the exact choice of μ is entirely arbitrary. We may now define g by substituting (2.20) into (2.19):

$$g^2(q) \approx g^2(\mu)[1 - I(\mu^2)]^{-1}[1 - I(q^2)] \tag{2.21}$$

where $g^2(\mu)$ may be defined by experiment and I is proportional to g_0^2 which, by (2.20) to first order, is equal to $g^2(\mu)$. So, expanding gives:

$$g^2(q) \approx g^2(\mu)[1 + I(\mu^2) - I(q^2) + O(g^4)], \tag{2.22}$$

and $g(q)$ is now a *renormalised* coupling. Now:

$$\begin{aligned} I(\mu^2) - I(q^2) &= \frac{-g^2}{2\pi^2}\int_0^1 \mathrm{d}z z(1-z) \\ &\quad \times\Big[\ln(\mu^2 z(1-z) - m^2) \\ &\quad - \ln(q^2 z(1-z) - m^2)\Big], \end{aligned} \tag{2.23}$$

so the divergent terms proportional to $2/\eta$ (recall (2.16))have cancelled and thus the definition of g^2 is now finite, as promised.

To $O(g^4)$, all we have done is add the *counter-term* $I(\mu^2)$ to the original definition of (g^2) (2.19). However, the cost of removing the indeterminacy of the divergent terms is an apparent dependence upon the choice of μ. Of course μ is arbitrary, so a physical quantity such as g cannot depend upon it. The solution to this quandary is in recognising that we may regard a variation in μ as instead a change in the scale of q. Consider the small m limit of (2.23):

$$I(\mu^2) - I(q^2) = \frac{-g^2}{\pi^2}\int_0^1 \mathrm{d}z z(1-z)\ln\left(\frac{\mu}{q}\right). \tag{2.24}$$

If we transform $\mu \to \mu e^z$, this is identical to $q \to q e^{-z}$ and it is now apparent that we should regard the coupling 'constant' g as being dependent upon the momentum transfered in a given reaction : g is a so-called *running* coupling. In effect, renormalization asserts that an empirically derived coupling will vary, depending upon the energy scale at which it is observed.[2]

2.2.3 Running couplings and the Renormalization Group.

The behaviour of running couplings now forms an important component of the search to understand more fundamental physics. The running behaviour is encapsulated in the Renormalization Group Equations (RGE's). In general these are a set of differential equations that link the variation of physical properties across the energy scale of a given theory. Thus they provide a means of extrapolating the predictions of a theory to (or from) experimentally accessible energies.

RGE's are derived from the independence of any physical property from a re-definition of μ, the Renormalisation Group (RG) itself being the group of transformations of μ. Among the RGE's is the so-called β-function which describes the running of a coupling and for the above example may be defined:

$$\beta(g) = \mu\frac{\partial g}{\partial \mu} = 0 \tag{2.25}$$

$$\approx \left[\sqrt{1 + I(\mu^2) - I(q^2)}\right]^{-1} \mu\frac{\partial}{\partial \mu}[I(\mu^2) - I(q^2)]. \tag{2.26}$$

What interests us here is the RG evolution of neutrino masses and mixings. In the SM, fermion mass is generated through the Yukawa coupling, h_f, of a fermion, f, to the Higgs scalar, $\phi =$. Due to spontaneous symmetry breaking at low energies, the scalar acquires a vacuum expectation value (VEV), v, which replaces ϕ in the Lagrangian, generating terms which are realised as masses, m_f. [30]

[2] This behaviour also applies to other fundamental properties such as the mass of particles and normalization of wave functions, to which renormalization will also apply.

$$
\begin{aligned}
\mathcal{L}_{\text{Mass}} &= h_f \bar{f}_R \phi f_L + h.c. && (2.27)\\
&= (vh_f)\bar{f}_R f_L + h.c. && (2.28)\\
& \quad m_f \bar{f}_R f_L + h.c. && (2.29)
\end{aligned}
$$

These couplings are responsible for the masses of the fermions and the composition of the mass eigenstates (i.e. the mixing matricies). As with the gauge couplings which transmit forces, the Yukawa couplings evolve according to the RG and this inevitably effects the mixing matricies. The RGE's that operate in the SM at one-loop level are due to Cheng, Eichten & Li [34]. Those for the Yukawa couplings are:

$$
\begin{aligned}
16\pi^2 \frac{\mathrm{d}}{\mathrm{d}t}\mathbf{Y}_U &= \Big(-\sum_{k=1}^{3}[c_U^k g_k^2] + \mathrm{Tr}[3\mathbf{Y}_U\mathbf{Y}_U^\dagger + 3\mathbf{Y}_D\mathbf{Y}_D^\dagger + \mathbf{Y}_E\mathbf{Y}_E^\dagger] \\
&\quad + \frac{3}{2}\mathbf{Y}_U\mathbf{Y}_U^\dagger - \frac{3}{2}\mathbf{Y}_D\mathbf{Y}_D^\dagger \Big)\mathbf{Y_U} && (2.30)\\
16\pi^2 \frac{\mathrm{d}}{\mathrm{d}t}\mathbf{Y}_D &= \Big(-\sum_{k=1}^{3}[c_D^k g_k^2] + \mathrm{Tr}[3\mathbf{Y}_U\mathbf{Y}_U^\dagger + 3\mathbf{Y}_D\mathbf{Y}_D^\dagger + \mathbf{Y}_E\mathbf{Y}_E^\dagger] \\
&\quad + \frac{3}{2}\mathbf{Y}_D\mathbf{Y}_D^\dagger - \frac{3}{2}\mathbf{Y}_U\mathbf{Y}_U^\dagger \Big)\mathbf{Y_D} && (2.31)\\
16\pi^2 \frac{\mathrm{d}}{\mathrm{d}t}\mathbf{Y}_E &= \Big(-\sum_{k=1}^{3}[c_E^k g_k^2] + \mathrm{Tr}[3\mathbf{Y}_U\mathbf{Y}_U^\dagger + 3\mathbf{Y}_D\mathbf{Y}_D^\dagger + \mathbf{Y}_E\mathbf{Y}_E^\dagger] \\
&\quad + \frac{3}{2}\mathbf{Y}_E\mathbf{E}_U^\dagger \Big)\mathbf{Y_E}, && (2.32)
\end{aligned}
$$

where $t = ln(\mu)$ and $\mathbf{Y}_F$ is the matrix of Yukawa couplings for each type of SM fermion, with components h_{ij}. F, the fermion type, can be any of E, U and D corresponding to charged leptons, up- and down-type quarks[3] ; i and j are species indicies corresponding to the individual members of one of the fermion types: e.g. $F = E$ allows $i, j = e, \mu, \tau$, however in this case (and $F = U$) the mass matrix is diagonal so that $i = j$. Also, there is dependence upon the gauge couplings g_k: $k = 1, 2, 3$ for the SM SU(k) gauge symmetries. c_F^k are summarized in Table 2.1. The gauge couplings evolve according to:

$$
16\pi^2 \frac{\mathrm{d}g_k}{\mathrm{d}t} = b_k g_k^3. \qquad (2.33)
$$

[3]Up-type are u, c & t; down-type are d, s & b.

F	k		
	1	2	3
E	15/4	9/4	0
U	17/2	9/4	8
D	5/12	9/4	8

Table 2.1: c_F^k in the Standard Model.

	k		
	1	2	3
b_k	41/6	24/43	-7

Table 2.2: b_k in the Standard Model.

Which yields analytical solutions:

$$g_k^2(t) = \frac{g_k^2(0)}{1 + b_k g_k^2(0)t}, \tag{2.34}$$

with b_k listed in Table 2.2.

The trace terms in (2.31)–(2.32) are due to the Yukawa equivalent of the vacuum polarisation diagram (recall 2.2) and the others are related to the various self-energy and vertex correction diagrams, some of which involve the gauge bosons.

A most intriguing result of the latter energy dependence is that the coupling strength of the three successfully quantised fundamental forces[4] tend to converge at some very large energy scale, though they do not meet at a single point.

Of course the neutrino should also be included now and especially at the scale of the right-handed neutrino mass, where the neutrino Yukawa coupling must surely be significant. But, at such vast energies we expect new physics to be in effect and the form of the RGE's will be altered as a consequence.

[4] Those that have been formulated as gauge theories.

2.3 Supersymmetry.

Considering the re-definition of the bare terms in the previous section, it is clearly unsatisfactory that there should be contributions to the bare Lagrangian that diverge as the regularization is removed. If the corrections are many orders of magnitude greater than the observed parameters, the fine cancellations between loops and counter-terms begin to look quite unnatural, a situation known as *fine-tuning*. But if the divergence is sufficiently weak, these contributions need not be troublesome. For instance, if the divergence of any diagram is only logarithmic, the corrections to the bare terms may be sufficiently small, even for very large values of a cut-off (or vanishing η in dimensional regularisation), that fine-tuning may be avoided. To achieve this, it is prudent to seek theories which inherently counter-act possible power-law divergences.

This is the case for Supersymmetry (SUSY). Here each of the known fermions of the SM has a bosonic counterpart. The rationale is that their is a relative minus sign between the correction due to a bosonic and a fermionic loop. Thus, with identical Yukawa couplings ensured by some deeper symmetry, these divergences are automatically cancelled, in much the same way as the Ward Identity insures the cancellation of the vertex correction and self-energy contributions to scattering.

In general SUSY introduces for every known fermion (boson) a bosonic (fermionic) counter-part and the related particles are grouped into chiral (vector) 'supermultiplets' [35]. SUSY is a symmetry under transformations within these supermultiplets and corresponds to replacing all fermions in the theory with their bosonic counterparts and vice versa. In pure SUSY the components of a supermultiplet share the same couplings and masses, ensuring the cancellation of the Higgs self energy quadratic divergence as mentioned above. But no scalar particle with a mass identical to any of the SM fermions has been detected, and so it is clear that this symmetry is broken, if it does indeed exist in nature. However at higher energies, where all particles begin to seem identically massless SUSY may well manifest itself.

It is thus in the high energy regime that we may assume SUSY to be a valid theory and use its structure to predict the renormalisation group evolution of physical properties to (or from) more fundamental energy scales.

An important additional feature of the SUSY model is the existence of two Higgs doublets. As the SM is defined, the Up-type fermions[5] couple directly with the only Higgs but, in order that the Yukawa couplings be gauge invariant, the Down-type fermions[6] must couple to the conjugate of the Higgs, $i\sigma_2 H^*$. However, requirements upon the form of the SUSY Lagrangian preclude this possibility and consequently SUSY features H_u and H_d which impart masses to the Up-[7] and Down-type fermions respectively. In general the VEV's, v_u and v_d, of the two Higgs will not be the same but are related to the effective VEV of the SM: $v = \sqrt{v_u^2 + v_d^2} = v\sqrt{\sin^2\beta + \cos^2\beta}$. Thus, an important parameter in SUSY models is $\tan\beta$ which is the ratio of the two VEV's. Its significance is that, because the masses of the known fermions and the SM VEV are known to reasonable accuracy, it translates into the relative sizes of Up- and Down-type Yukawa couplings.

This is essential knowledge in studies of RG evolution within the context of SUSY which represents the only existing means of connecting the latter's predictions with experiment. furthermore, particular variations of SUSY prefer specific ranges of $\tan\beta$ and overall it may vary from $\sim$1 to $\sim$60.[8] For instance, certain boundary conditions, such as $h_\tau = h_b = h_t$, require $\tan\beta$ to be large.

We are specifically interested here in the evolution of the Yukawa couplings, whose one-loop RGE's in SUSY are listed by Grzadkowski, Lindner & Theisen [36]:

---

[5]Up-type quarks only, in the SM.

[6]Down-type quarks and charged leptons.

[7]Up-type quarks and now also neutrinos.

[8]$\tan\beta$ tends to be larger than one in order to accomadate the fact that the top-type quark masses tend to be larger than the down-type's.

	k		
	1	2	3
b_k	11	1	-3

Table 2.3: b_k in supersymmetric models.

$$16\pi^2 \frac{\mathrm{d}}{\mathrm{d}t}\mathbf{Y}_U = \Big(-\sum_{k=1}^{3}[c_U^k g_k^2] + \mathrm{Tr}[3\mathbf{Y}_U\mathbf{Y}_U^\dagger + \mathbf{Y}_N\mathbf{Y}_N^\dagger] + 3\mathbf{Y}_U\mathbf{Y}_U^\dagger + \mathbf{Y}_D\mathbf{Y}_D^\dagger\Big)\mathbf{Y_U} \tag{2.35}$$

$$16\pi^2 \frac{\mathrm{d}}{\mathrm{d}t}\mathbf{Y}_D = \Big(-\sum_{k=1}^{3}[c_D^k g_k^2] + \mathrm{Tr}[3\mathbf{Y}_D\mathbf{Y}_D^\dagger + \mathbf{Y}_E\mathbf{Y}_E^\dagger] + 3\mathbf{Y}_D\mathbf{Y}_D^\dagger + \mathbf{Y}_U\mathbf{Y}_U^\dagger\Big)\mathbf{Y_D} \tag{2.36}$$

$$16\pi^2 \frac{\mathrm{d}}{\mathrm{d}t}\mathbf{Y}_N = \Big(-\sum_{k=1}^{3}[c_N^k g_k^2] + \mathrm{Tr}[3\mathbf{Y}_U\mathbf{Y}_U^\dagger + \mathbf{Y}_N\mathbf{Y}_N^\dagger] + 3\mathbf{Y}_N\mathbf{Y}_N^\dagger + \mathbf{Y}_E\mathbf{Y}_E^\dagger\Big)\mathbf{Y_N} \tag{2.37}$$

$$16\pi^2 \frac{\mathrm{d}}{\mathrm{d}t}\mathbf{Y}_E = \Big(-\sum_{k=1}^{3}[c_E^k g_k^2] + \mathrm{Tr}[3\mathbf{Y}_D\mathbf{Y}_D^\dagger + \mathbf{Y}_E\mathbf{Y}_E^\dagger] + 3\mathbf{Y}_E\mathbf{E}_U^\dagger\Big)\mathbf{Y_E}, \tag{2.38}$$

where the neutrino has been included as F=N. The gauge couplings still evolve according to 2.33 and 2.34. Though the coefficients b_k have changed: see Table 2.3.

In comparison to the SM RGE's, we may note differences in the structure of the trace terms, where their arguements have been segregated into Up- and Down-type Yukawa couplings due to the exclusive coupling of the two Higgs. Also, the relative strengths of the gauge couplings have been altered: see Table 2.4.

The latter is a feature of SUSY which greatly improves the convergence of the gauge couplings at high energies: a state known as unification. Beyond this there are schemes in which the Yukawa couplings too are unified. Such theories which promise to unite many apparently disparate couplings are

F	k		
	1	2	3
E	3	3	0
N	1	3	0
U	13/9	3	16/3
D	7/9	3	16/3

Table 2.4: c_F^k in supersymmetric models.

refered to as Grand Unified Theories (GUT). Another promising feature is the robustness of predictions of the top mass, which correponds to an infrared fixed point of the theory. That is to say, the value of the top mass varies little across many variations of the theory.

SUSY is thus a promising candidate for a deeper theory, going beyond the SM but remaining in touch with some of its features. It comprises a suitable background in which to model the physics of the right-handed neutrino, and hence of neutrino mass, as it is envisaged in the see-saw mechanism. Using this background we can hope to translate the relationships that are possibly realised at very great energies into predictions of behaviour at experimentally accessible ones.

Chapter 3

Application.

Renormalisation parameters for the neutrino sector, a possible texture and how it compares to the experimental situation.

3.1 Renormalisation of See-saw scale symmetries.

Following Ellis & Lola [37] we assume some simple fundamental texture of the neutrino mass martrix to exist at a scale appropriate to the right-handed neutrino mass, M_R, in see-saw schemes. In a background of SUSY dynamics, renormalisation effects will rotate this texture as it is observed at some lower scale,M_{SUSY} , where SUSY gives way to the SM.

We note that below M_R the Dirac-character neutrino Yukawa couplings are integrated out, leaving the effective neutrino mass matrix, $\mathbf{M}'$, which evolves according to:

$$\begin{aligned} 8\pi^2\frac{\mathrm{d}}{\mathrm{d}t}\mathbf{M}' &= \Big(-c^k g_k^2 + \mathrm{Tr}[3\mathbf{Y}_U\mathbf{Y}_U^\dagger]\Big)\mathbf{M}' \\ &\quad+\frac{1}{2}\Big((\mathbf{Y}_E\mathbf{Y}_E^\dagger)\mathbf{M}' + \mathbf{M}'(\mathbf{Y}_E\mathbf{Y}_E^\dagger)^T\Big) \end{aligned} \tag{3.1}$$

Where, for clarity, the sum over k is implied. Assuming that the trace across the up-type quark Yukawa couplings is dominated by the third generation (i.e. the top), we may recast (3.1) in component form:

$$\frac{1}{M'_{ij}}\frac{\mathrm{d}}{\mathrm{d}t}M'_{ij} = \frac{1}{8\pi^2}\Big(c^k g_k^2 + 3h_t^2 + \frac{1}{2}(h_i^2+h_j^2)\Big) \tag{3.2}$$

$$= A. \tag{3.3}$$

Where $i, j = e, \mu, \tau$. To determine the effect of the RG evolution, we may integrate between the scale at which we define the matrix, $t_0 = \ln M_R/M_R$, and the scale close to that at which we currently make observations, $t_1 = \ln M_{SUSY}/M_R$.

$$\int_{t_0}^{t_1}\frac{1}{M'_{ij}}\mathrm{d}M'_{ij} = \int_{t_0}^{t_1} A\mathrm{d}t \tag{3.4}$$

$$\int_{t_0}^{t_1}\mathrm{d}(\ln M'_{ij}) = \int_{t_0}^{t_1} A\mathrm{d}t \tag{3.5}$$

$$\ln(M'(t_1))_{ij} - \ln(M'(t_0))_{ij} = \int_{t_0}^{t_1} A\mathrm{d}t \tag{3.6}$$

$$\frac{(M'(t_1))_{ij}}{m'_{ij}} = e^{\frac{1}{8\pi^2}\left[\int_{t_0}^{t_1} c^k g_k^2 + 3h_t^2 + \frac{1}{2}(h_i^2+h_j^2)\mathrm{d}t.\right]} \tag{3.7}$$

Where $\mathbf{m}' = \mathbf{M}'(t_0)$. One-loop renormalisation effects may thus be characterised according to:

$$\left.\begin{array}{rcl} I_g & = & e^{\frac{1}{8\pi^2}\int_{t_0}^{t_1} c^k g_k^2 \mathrm{d}t} \\ I_t & = & e^{\frac{1}{8\pi^2}\int_{t_0}^{t_1} h_t^2 \mathrm{d}t} \\ I_j & = & e^{\frac{1}{8\pi^2}\int_{t_0}^{t_1} h_j^2 \mathrm{d}t} \end{array}\right\} \tag{3.8}$$

I_j generally will be less than one and the most prominent effect is in the third generation as h_τ is the greatest of the three. The first generation is essentially unaffected and I_e is close to one.

Now:

$$\frac{M'(t_1)_{ij}}{m'_{ij}} = I_g I_t^3 \sqrt{I_i I_j}. \tag{3.9}$$

Thus we may define the RG-evolved effective neutrino mass matrix:

$$\mathbf{M}'(t_1) = I_g I_t^3 \times \begin{pmatrix} m'_{ee} I_e & m'_{e\mu}\sqrt{I_e I_\mu} & m'_{e\tau}\sqrt{I_e I_\tau} \\ m'_{\mu e}\sqrt{I_\mu I_e} & m'_{\mu\mu} I_\mu & m'_{\mu\tau}\sqrt{I_\mu I_\tau} \\ m'_{\tau e}\sqrt{I_\tau I_e} & m'_{\tau\mu}\sqrt{I_\tau I_\mu} & m'_{\tau\tau} I_\tau \end{pmatrix} \tag{3.10}$$

Ellis & Lola have calculated I_j for $M_R = 10^{13}$GeV, $M_{SUSY} = 1$TeV and a specific set of initial values of h_τ: in effect, a range of $\tan\beta$. The results are tabulated below (Table 3.1) with the ratio I_τ/I_μ, whose significance will be explained in the following section. The left-hand side of the table contains selected results from Table 1 (p.8) of [37]; the right-hand side contains estimates of the correlation with $\tan\beta$ which are the authors own, except for the least and greatest which are noted in [37]. The author has attempted to

h_τ	I_τ	I_μ	I_τ/I_μ	$\tan\beta$
3.0	0.826	0.9955	0.8297	58.2
1.2	0.873	0.9981	0.8747	~ 55
0.48	0.9497	0.9994	0.9503	~ 40
0.10	0.997	0.99997	0.9970	~ 13
0.013	0.99997	1.00000	0.99997	1.0

Table 3.1: I_τ and I_μ with approximate values of $\tan\beta$.

replicate these results in order to relate more reliably $\tan\beta$ to h_τ, and hence I_τ/I_μ, in the intermediate range. However, the author acquired consistently smaller values for both I_τ and I_μ and thus defers to [37].

3.2 Constraints from a simple See-saw scale neutrino symmetry.

Some symmetry of the neutrino mass matrix is assumed to exist at the see-saw scale, where right-handed neutrinos acquire a (huge) mass. A symmetry will impose specific constraints on the mixing parameters which characterise the texture. Such constraints should simplify interpretation of the matrix by inter-relating the mixing parameters.

As discussed above, renormalisation effects will rotate the mass matrix to some extent, such that the symmetry realised at high energies is no longer exact at experimental energies. Consequently, the symmetry constraints will be somewhat weakened.

Our task is to determine whether the constraints due to a given symmetry are consistent with the experimentally determined values of the mixing parameters. We will compare the empirically derived mass matrix with the renormalisation-group-distorted form of a chosen see-saw scale symmetric mass matrix, henceforth the RG-matrix.

We assume the RG-matrix to be correct and use it as a theoretical basis in which to inter-relate the mixing parameters and thereby predict the experimentally less certain parameters from others, which are known with more accuracy. A comparison of these predictions to the experimentally allowed region is an effective measure of the feasibility of this model. Furthermore, it is instructive to analyse the variation of the predictions as the input values are varied across their experimentally allowed regions.

3.2.1 Symmetry relations.

After Lam [29], we begin by assuming that there exists, at the scale of the right-handed neutrino mass, an exchange symmetry between the second and third generations in the neutrino mass matrix, $\mathbf{m}'$. The neutrino mass matrix is expressed in the mass-diagonal basis of the charged leptons, such that:

$$\mathbf{m}' = \mathbf{u}\mathbf{m}\mathbf{u}^T, \tag{3.11}$$

where $\mathbf{m}$ is the diagonal matrix of neutrino mass eigenvalues and $\mathbf{u}$ is the MNS matrix as defined in (1.8)

This so-called 2-3 symmetry requires:

$$\left.\begin{array}{rcl} m'_{e\mu} & = & -m'_{e\tau} \\ m'_{\mu\mu} & = & m'_{\tau\tau} \end{array}\right\} \tag{3.12}$$

The minus sign in the first expression is necessary to maintain the convention of positive mixing angles. In order to fulfill these relations $\mathbf{m}'$ contains four free parameters and takes the form:

$$\mathbf{m}' = \begin{pmatrix} a & b & -b \\ b & f & e \\ -b & e & f \end{pmatrix} \tag{3.13}$$

with eigenvalues $f+e$ and $\frac{1}{2}[f-e+a\pm\sqrt{(f-e-a)^2+8b^2}]$. This fixes the MNS matrix to the form:

$$\mathbf{u} = \begin{pmatrix} c_1 & s_1 & 0 \\ -\frac{1}{\sqrt{2}}s_1 & \frac{1}{\sqrt{2}}c_1 & \frac{1}{\sqrt{2}} \\ \frac{1}{\sqrt{2}}s_1 & -\frac{1}{\sqrt{2}}c_1 & \frac{1}{\sqrt{2}} \end{pmatrix}, \tag{3.14}$$

and the solar mixing angle, $\theta_{12} = \theta_1$, will be a positive solution of $\cot\theta_{12} = [f-e-a\pm\sqrt{(f-e-a)^2+8b^2}]/2\sqrt{2}b$.

Thus the exact symmetry makes no demands upon either the mass spectrum or the solar mixing angle as these may be accomadated with a suitable definition of the four free parameters in (3.13).

By comparing (3.14) with (1.24) we may note that this symmetry fixes the 2-3 mixing angle ($\theta_{23} = \theta_2$) as exactly $\pi/4$: a state of maximal mixing. Also, the 1-3 mixing angle ($\theta_{13} = \theta_3$) must be exactly zero. These predictions are in agreement with the current results of neutrino oscillation experiments, but as we have seen the texture of the matrix will evolve according to the RGE's, somewhat loosening these restrictions but also inter-relating the constrained parameters with those that remain indeterminate under the exact symmetry.

Applying the RGE's, as in the previous section, the symmetric matrix is distorted as it is observed at the scale $t = t_1$:

$$\mathbf{m}' = \mathbf{M}'(t_0) \rightarrow \mathbf{M}'(t_1) \tag{3.15}$$

Scenario.	Parameter.	
	$\tan^2\theta$	Δm^2 (eV^2)
Atmospheric	1.6	3.0×10^{-3}
LMA	0.4	3.0×10^{-5}
LOW	0.8	1.0×10^{-7}

Table 3.2: Original best-fit values of the oscilation parameters [38].

and the symmetry requirements may be re-cast in terms of (3.10) as:

$$\left(\frac{M'_{e\tau}}{M'_{e\mu}}\right)^2 = \frac{M_{\tau\tau'}}{M'_{\mu\mu}} = \frac{I_\tau}{I_\mu} \tag{3.16}$$

The right-most expression, henceforth $\frac{I_\tau}{I_\mu} = R$, follows directly from (3.10) and is dependent upon $\tan\beta$: it ranges from 0.8297, corresponding to $\tan\beta = 58.2$, to 0.99997, for $\tan\beta = 1$ (Table 3.1). It characterises the strength of the RG effects and will be exactly one in the absence of them: deviation from 1 is an indication of RG evolution. The other two expressions are complicated functions of the the mixing angles and masses, or, equivalently, the mixing angles, mass differences and least mass, m_0.

The approach of [29] was to fulfill the first equality of (3.16) and then determine the appropriate value of R. This relation was formulated in terms of the experimental best-fits for the solar and atmospheric mixing parameters, as presented in [38] and repeated here for convenience (see Table 3.2), and a value of the least mass between 0 and 2eV, in keeping with the tritium β-decay results. Then the veracity of this relation was tested for t_3 below the CHOOZ limit. If the first relation could be satisfied the second was used to determine R which was finally compared to the limits imposed by Ellis & Lola.

An interesting result was that the symmetry relations (3.16) could not be reconciled with the limits on R when the least mass was less than approximately 0.025eV. In effect the symmetry is incompatible with a least mass below this value, if the renormalization effects are indeed accounted for by SUSY dynamics.

Since the publication of [29], new experimental data ([24], [26]) has altered the best-fit values of the oscillation parameters which were used as inputs for this study. The new values are listed in Table 1.1. Here we take the opportunity to explicitly update the minimum allowed least mass for the LOW and LMA scenarios, see Table 3.3. Experimental developments now effectively rule out the SMA scenario. We note that the lower bound on m_0

Scenario	m_0(eV)	$\tan^2\theta_3$	I_τ/I_μ
LMA	0.01507	0.2753	0.829724
	0.0431	0.02633	0.92852
LOW	0.01614	0.5758×10^{-6}	0.829687

Table 3.3: Revised values for the lower limit of m_0.

due to I_τ/I_μ has decreased somewhat and that the associated value of $\tan^2\theta_3$ is considerably larger in both scenarios. In fact, it exceeds the CHOOZ boundary of $\tan^2\theta_3 < 0.026$ by an order of magnitude in the LMA. As a result, in the latter case it is actually the CHOOZ boundary which imposes the lower limit upon m_0 and so, simultaneously, a lower limit upon I_τ/I_μ.

3.2.2 Global analysis.

We now seek to extend the work of [29] by considering the case that the symmetry relations (3.16) may be fixed using input values removed from the experimental best-fit. As we have seen in Section 1.2.3, neutrino oscillation experiments have succeeded in determining allowed regions surrounding the best-fit points in the parameter space of the neutrino mass matrix. To a greater or lesser degree, anywhere within these regions could explain the observed behaviour of neutrino fluxes. The degree of certainty to which a point in the parameter space agrees with experiment is marked by the Confidence Level (CL). Thus the parameter space is divided by CL boundaries, within which it can be stated, with a given CL, that the true value of the parameters is located.

The solar and atmospheric parameters (one mixing angle and one mass-squared difference each) are confined to closed regions by the CL boundaries. The solar and atmospheric results thus provide us with definite ranges for four of the parameters: θ_1, Δm^2_{21}, θ_2 and Δm^2_{32}. The remaining mixing angle, θ_3, and mass, m_0, are restricted only by an upper bound. In the context of this model, the symmetry relations will now impose additional limits on these two parameters.

By requiring:

$$\begin{aligned} 0 &= \left(\frac{M'_{e\tau}}{M'_{e\mu}}\right)^2 - \frac{M_{\tau\tau'}}{M'_{\mu\mu}} && (3.17) \\ &= R_1 - R_2, && (3.18) \end{aligned}$$

and expressing this relation using values culled from the allowed regions of the solar and atmospheric parameters, we obtain an expression in θ_3 and m_0. We may select a value of θ_3 (m_0) and solve numerically for m_0 (θ_3). To determine the accompanying value of R we may simply substitute the solution so obtained into either R_1 or R_2.

The exact form of (3.18) depends upon the mass hierarchy used. In much of the following we assume that the neutrino mass spectrum obeys the normal hierarchy:

$$m_1 = m_0 < m_2 = \sqrt{m_0^2 + \Delta m^2_{21}} < m_3 = \sqrt{m_0^2 + \Delta m^2_{21} + \Delta m^2_{32}}. \quad (3.19)$$

This assumption follows from [29] where it was shown that the inverted hierarchy:

$$m_3 = m_0 < m_1 = \sqrt{m_0^2 - \Delta m^2_{32} - \Delta m^2_{21}} < m_2 = \sqrt{m_0^2 - \Delta m^2_{32}}, \quad (3.20)$$

where $\Delta m^2_{32} < 0$, cannot satisfy the bounds on R. Specifically, it can be shown that, for the best-fit values of the atmospheric and solar parameters, the inverted hierarchy yields $R > 1$ in this model, which is disallowed by the assumption that $M_{SUSY} < M_{RH}$, as may be seen from the structure of I_τ and I_μ (3.8), which demands the maximum value of R cannot exceed 1.

The interdependence of the three parameters under (3.18), for the best-fit values of Table 1.1, is shown in Fig. 3.1 for the LMA scenario and in Fig. 3.2

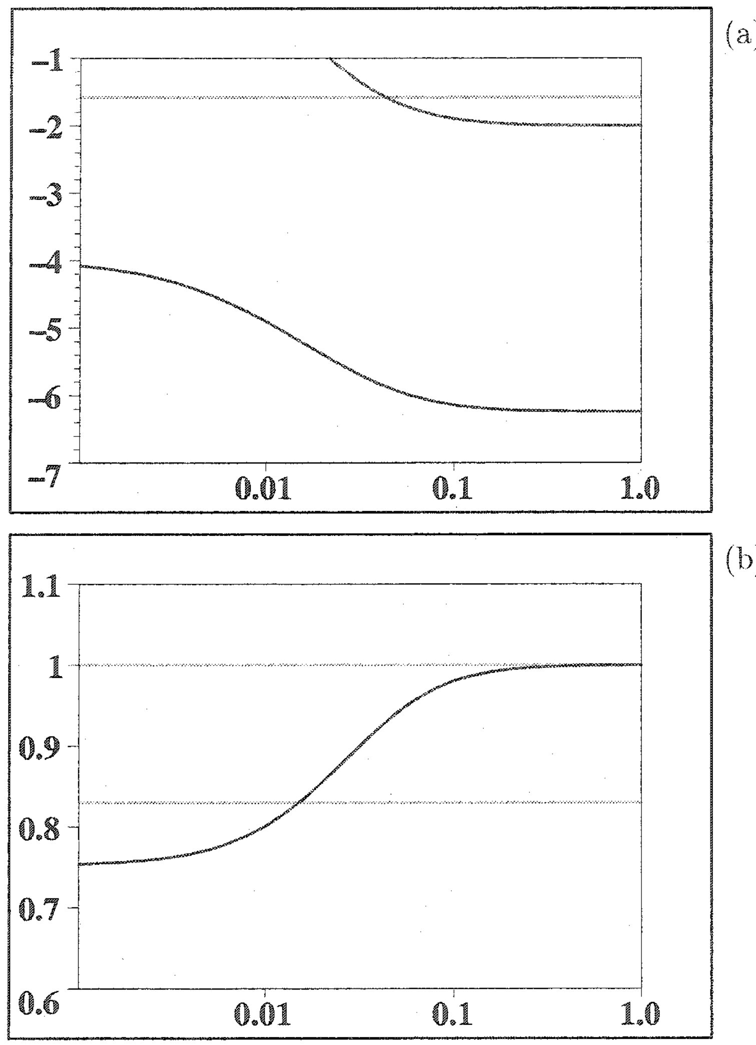

Figure 3.1: Behaviour of (a) $\log t_3^2$ and (b) R against m_0/eV in the LMA scenario.

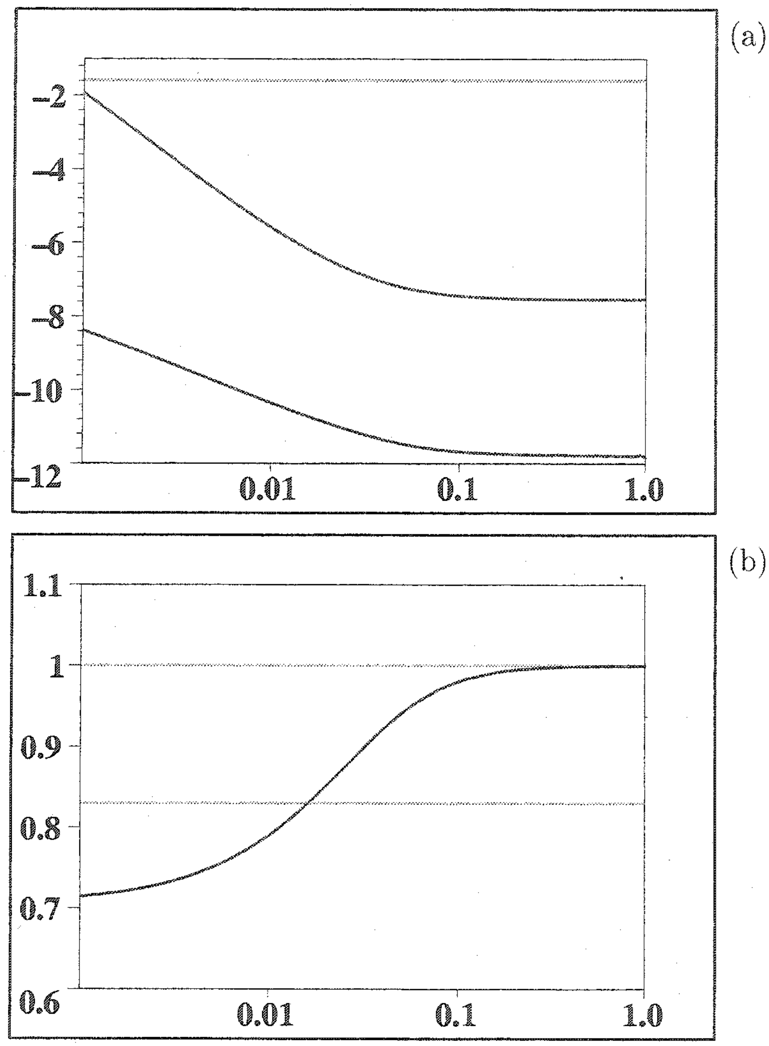

Figure 3.2: Behaviour of (a) $\log t_3^2$ and (b) R against m_0/eV in the LOW scenario.

for the LOW scenario. The upper panel in each figure shows $\log t_3^2$ against m_0 with the CHOOZ boundary of $t_3^2 < 0.026$ (90% CL) marked; the lower panel of each shows R against m_0 with the upper and lower limits on R, 0.8297 and 0.99997 respectively.

An interesting feature is that here we have two distinct solutions in $\tan^2\theta_3 = t_3^2$ for both scenarios. These correspond to positive and negative values of θ_3. Although, by definition, $0 < \theta_3 < \pi/2$ these two solutions are still allowed because the Dirac phase, δ, in (1.24) appears always and only in conjunction with $\sin\theta_3$. Thus, the apparent $\theta_3 < 0$ solutions may instead be associated with the case of $\delta = \pi$ and so maintain $\theta_3 > 0$. We find the latter case reproduces the results of [29] when using the data of Table 3.2. Note that R is plotted for both solutions in each of the two scenarios but the curves overlap as to be indistinguishable.

We are faced with four cases consisting of two solutions, $+$ and $-$ (for $\theta_3 > 0$ and $\theta_3 < 0$ respectively), in each of the two scenarios, LMA and LOW. Each case, henceforth, may be refered to individually as (LMA, $+$), (LMA, $-$), (LOW, $+$) and (LOW, $-$); or they may be grouped into both LMA [LOW] solutions as (LMA, $\pm$) [(LOW, $\pm$)], or into the $+$ [$-$] solutions of both scanarios as (L, $+$) [(L, $-$)].

We may note several general trends:

- t_3^2 decreases for increasing m_0 in all cases.
- t_3^2 is asymptotic to a minimum value at large m_0 in all cases.
- t_3^2 is somewhat larger for (LMA, $-$) [(LOW, $-$)] compared to (LMA, $+$) [(LOW, $+$)].
- t_3^2 is significantly larger for (LMA, $+$) [(LMA, $-$)] compared to (LOW, $+$) [(LOW, $-$)]
- R behaves identically for both solutions of (LMA, $\pm$) or (LOW, $\pm$): it increases with m_0 and is asymptotic to 1 at large m_0.

The last point may be understood in terms of the increasing value of m_0 diluting the effects of the mass differences as the mass spectrum tends towards degeneracy. The original symmetry (3.12) exhibits complete freedom in the mass spectrum, as is seen in the eigenvalues of (3.13). A completely non-degenerate spectrum will require all four of the parameters in (3.13) to be defined, whereas a completely degenerate spectrum requires only f and e. In this sense there is more freedom in the degenerate case and so it is closer to a state compatibile with the original symmetry and in conjunction with this the renormalization effects must be weaker and therefore R closer to 1.

It is interesting to note that t_3 does not approach zero. In comparison to the resolution of modern experiment, which prefers $\theta_3 = 6°$ ($t_3^2 = 0.011$) but with no statistical weight over $\theta_3 = 0$ [26], the range of t_3^2 for all solutions, except (LMA, $-$), is easily consistent with zero, which is a prediction of the original symmetry. However, renormalization running explicitly breaks the symmetry and prevents t_3 from reaching exactly zero.

The (L, $-$) solutions exceed the CHOOZ boundary for sufficiently small m_0. However, for (LOW, $-$) the lower R bound is reached before this occurs. These factors are the origin of the exclusion of $m_0 = 0$ in [29]. Returning to the results of Table 3.3, we recall that (LMA, $-$) violates the CHOOZ boundary for $m_0 < 0.0431$ which corresponds to $R < 0.92852$. Comparing this relation to Table 3.1, we note that this implies that (LMA, $-$), at the best-fit point of the existing experimental data, is incompatible with $\tan\beta \gtrsim 45$.

Of interest too are the constraints on R imposed by the upper bounds upon m_0. There is a selection of upper bounds on m_0 from tritium (^3_1H) *beta*-decay [3] and $2\beta0\nu$ [4] and we tabulate R against these limits in Table 3.4. For larger values of m_0 discrepancies between (LMA, $\pm$) and (LOW, $\pm$)

Scenario.	Upper Bound.		
	$2\beta0\nu$ 68% CL	$2\beta0\nu$ 90% CL	^3_1H 90% CL
	0.26eV	0.34eV	2.2eV
LMA	0.99671	0.99806	0.99995
LOW	0.99673	0.99807	0.99995

Table 3.4: Upper limits on R due to large mass constraints on the neutrino.

are reduced and at each of these limits the corresponding values of R are very similar between the scenarios. The tritium β-decay bound allows R to be as large as 0.99995 which is very close to the theoretical maximum of 0.99997. The $2\beta0\nu$ bounds are more restrictive and require $R \lesssim 0.997$ which may be interpreted as $\tan\beta \gtrsim 13$. Although, the tritium β-decay result is the more trustworthy, the $2\beta0\nu$ bounds do demonstrate the potential of the model for placing limits upon the choice of $\tan\beta$. This will be more relevant when the next generation of tritium β-decay experiments [2], which aim to probe the sub-eV domain, begin to take data.

The behaviour described above is in the case of the best-fit values of the solar and atmospheric oscillation parameters. For the most part the general properties will remain unaltered as the input values depart from this ideal case. However, details such as the asymptotic value of t_3^2 or the exact values at which certain boundaries are crossed will vary.

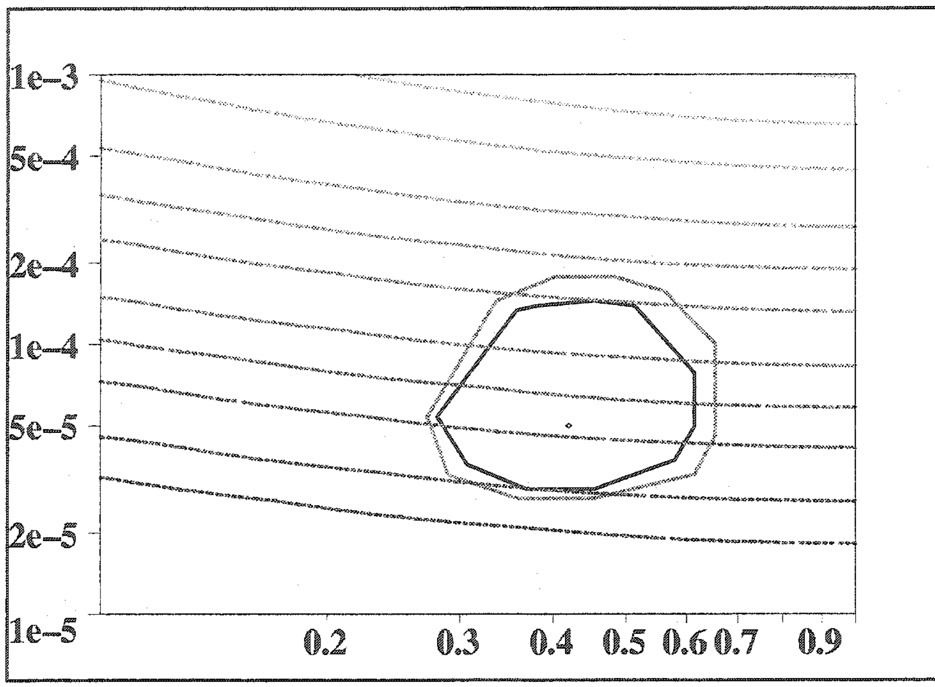

Figure 3.3: Contours (broken) of $(+t_3)^2$ =0.1, 0.2, 0.5, 1.0, 2.0, 5.0, 10, 20, 50, 100, 200$\times10^{-6}$ for m_0 = 0.26eV in the space of solar parameters ($\Delta m_{21}^2/\text{eV}^2$ against t_1^2) around the LMA region (90, 95%CL).

3.2.3 Space of solar parameters.

Firstly we will examine the dependence of the model upon the solar parameters. We determine how the model varies across the space of solar parameters, keeping the atmospheric ones fixed at the best-fit. It is obvious from the different specific behaviours of the two solar scenarios that there is some dependence upon the solar parameters. This dependence is illustrated in Fig. 3.3 and Fig. 3.4, which show contours of t_3^2 in relation to the LMA region of the solar parameter space.

Generally, the model turns out to have only very slight dependence upon t_1, which is a consequence of θ_1 being undetermined by the exact symmetry, before RG effects are taken into account. More significant is the dependence

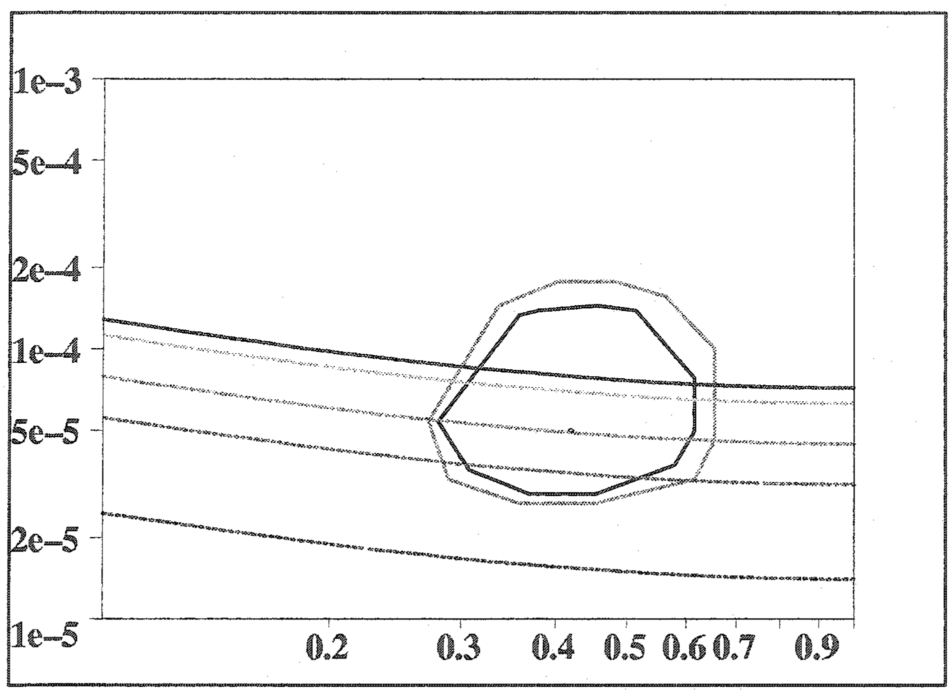

Figure 3.4: Contours of $(-t_3)^2$ =0.001, 0.002, 0.005, 0.01, 0.02 (broken) and 0.026 (solid) for $m_0 = 0.26\text{eV}$ in the space of solar parameters ($\Delta m^2_{21}/\text{eV}^2$ against t_1^2) around the LMA region (90, 95%CL).

upon Δm^2_{21}, which essentially accounts for all differences between the two solar mixing scenarios. We note that, for fixed m_0, t_3^2 and R both increase with increasing Δm^2_{21}, though R varies very slowly.

Fig. 3.3 shows contours of t_3^2 for $m_0 = 0.26$eV which is the upper limit (68%CL) on m_0 from the Heidelberg-Moscow experiment. These contours represent the solution of $t_3 > 0$. They are superimposed upon the vicinity of the LMA scenario, the allowed region of which is indicated at 90 and 95% CL by the closed curves (inner and outer respectively) which surround the best-fit marked by a diamond. Between the 90%CL boundaries t_3^2 varies between 0.2×10^{-6} and 5.0×10^{-6}. Although this is more than an order of magnitude, the entire range is easily consistent with existing limits on t_3, as was discussed previously, and cannot be tested in the forseeable future.

Fig. 3.4 likewise shows contours of t_3^2 for $m_0 = 0.26$eV . Here, however, the solution of $t_3 < 0$ is represented. Overall the trend is very similar but, as expected, t_3^2 is much larger. In fact it exceeds the CHOOZ boundary (solid curve) in the large Δm^2_{21} part of the LMA region. The 90 and 95% CL boundaries shown are calculated in [24] under the assumption that $t_3 = 0$. However, studies such as [26] indicate that the LMA region is altered little even for t_3^2 as great as 0.05 [26] and so it is still reasonable to compare the LMA boundaries shown with the contours, even up to the CHOOZ boundary. With this value of m_0, all $\Delta m^2_{21} > 8.32 \times 10^{-5}$ within the LMA 95%CL boundary are excluded by the CHOOZ limit. A larger value of m_0 makes little difference to the position of the CHOOZ boundary. On the other hand, if m_0 were smaller t_3^2 would be boosted and the CHOOZ boundary would migrate towards smaller Δm^2_{21}, eventually encompassing the best-fit point. This is the origin of (LMA, $-$) exceeding the CHOOZ boundary.

3.2.4 Space of atmospheric parameters.

Now we turn to the atmospheric parameters. We keep the solar parameters fixed at their best-fit values and examine the behaviour of the model for variations in Δm^2_{32} and t_3^2.

Here the dependence upon the mass-squared difference, Δm_{32}^2, is the more simple of the two parameters. As it increases, for fixed m_0, t_3^2 and R are both suppressed. Again, in this model moving away from degeneracy is tied to stronger RG effects (smaller R).

Behaviour at $\tan\theta_2 = 1$.

The dependence upon the mixing angle, t_2^2, presents special circumstances. R depends more strongly upon t_2^2 than on the other parameters and as the latter falls, with fixed m_0, R increases. Now, when $\theta_2 = \pi/4$ there is exactly maximal mixing between the second and third generations, which is a prediction of the symmetric matrix *before* RG effects are introduced. Thus, this corresponds to the case of no RG evolution so that $R = 1$ when $t_2^2 = 1$ no matter the values of the other parameters. Crucially, this means that $R > 1$ for all $t_2^2 < 1$ (see Fig. 3.5) and this region, which represents up to half of the *experimentally allowed* atmospheric parameter space, is forbidden by the model.

This raises the spectre of the inverted hierarchy which, we recall, was disallowed by the upper bound on R for the case of best-fit values as inputs.

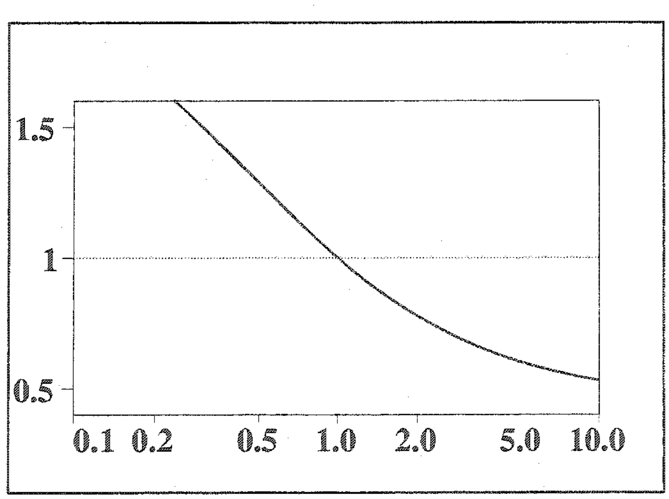

Figure 3.5: R against t_2^2: $R > 1$ for $t_2^2 < 1$, under the normal hierarchy.

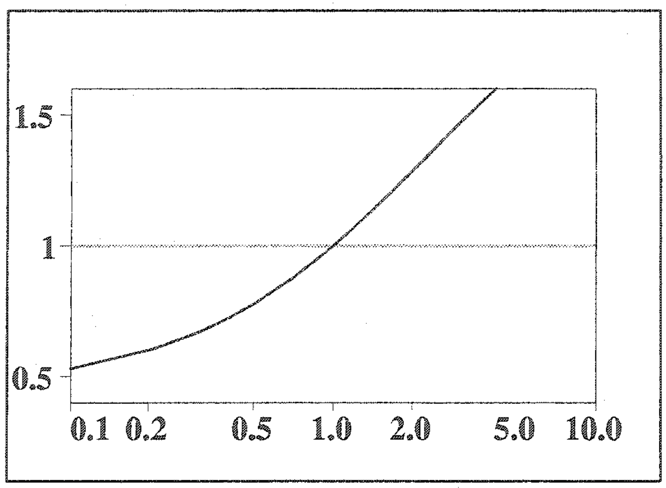

Figure 3.6: R against t_2^2: $R > 1$ for $t_2^2 > 1$, under the inverted hierarchy.

But it is reasonable to assume that if $(R-1)$ changes sign at $t_2^2 = 1$ for the normal hierarchy the same will be true for the inverted, and so there will be an allowed region for the latter where $t_2^2 < 1$. This is indeed the case, as is seen in Fig. 3.6, but we will not study this region in detail as it excludes the best-fit value.

Now, in the limit of vanishing θ_3, where solar and atmospheric mixing decouple, the experimentally allowed region in the atmospheric parameter space is symmetrical about $t_2^2 = 1$ because two neutrino vacuum oscillations depend upon $\sin^2 2\theta$, which is symmetrical about $\theta = \pi/4$. With this in mind, it is interesting that this model predicts small θ_3 but also excludes one of the resulting redundant regions of the parameter space. We will examine this a little more closely in the conclusion.

The behaviour of t_3 at $t_2 = 1$ is also noteworthy. One might now expect that with $t_2 = 1$ recreating the exact symmetry, we would find that it coincides with $t_3 = 0$. This is not quite true. As we approach $t_2 = 1$ from large t_2 the behaviour of t_3 is quite different between (L, +) and (L, −) (see Fig. 3.7 and Fig. 3.8 respectively). In the former case t_3^2 drops towards zero

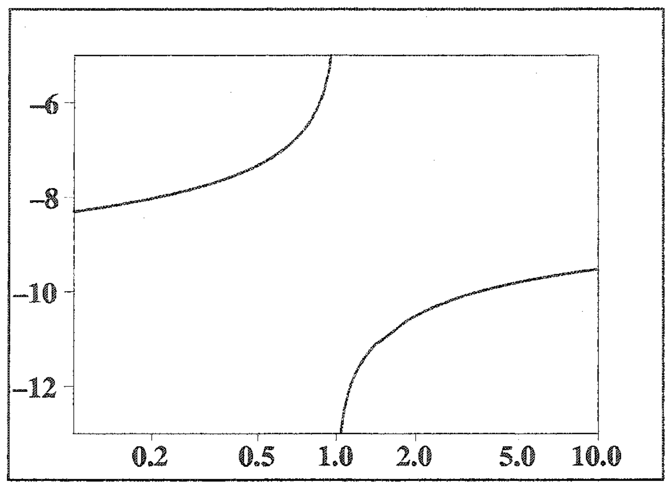

Figure 3.7: $\log((+t_3)^2)$ against t_2^2 across $t_2^2 = 1$.

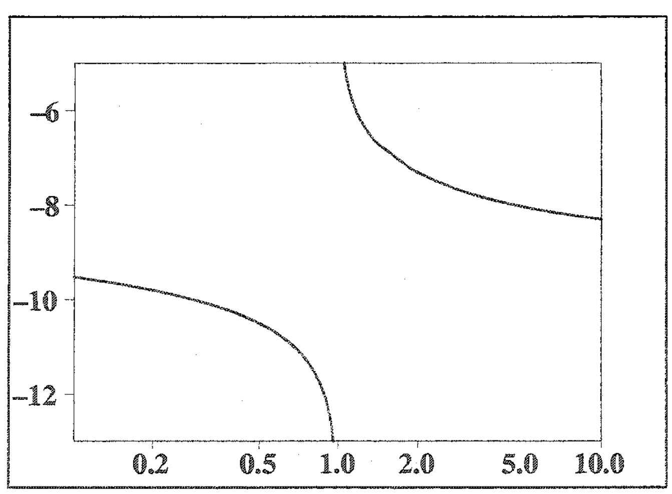

Figure 3.8: $\log((-t_3)^2)$ against t_2^2 across $t_2^2 = 1$.

and in the latter it actually diverges. But, when approaching $t_2 = 1$ from small t_2, the rôles are reversed. Thus, at exactly $t_2 = 1$, t_3^2 is ill-defined and consistent with zero.

Behaviour in the full parameter space.

The distinct behaviours of (L, +) and (L, −) around $t_2^2 = 1$ lead to quite different trends across the full parameter space as shown in Fig. 3.9 and Fig. 3.10. Note that, following the previous discussion, we have discarded the $R > 1$ region which also avoids the divergence of t_3 for (L, −).

Fig. 3.9 shows contours of t_3^2 for the $t_3 > 0$ solution, superimposed upon the experimentally allowed region. In accordance with our previous observations, $t_3^2 = 0$ at $t_2^2 = 1$ and it is apparent that t_3 is easily consistent with zero across the entire displayed area of the parameter space. Thus the 90 and 95% CL boundaries shown here (the closed curves) are those calculated in [26] at $t_3 = 0$.

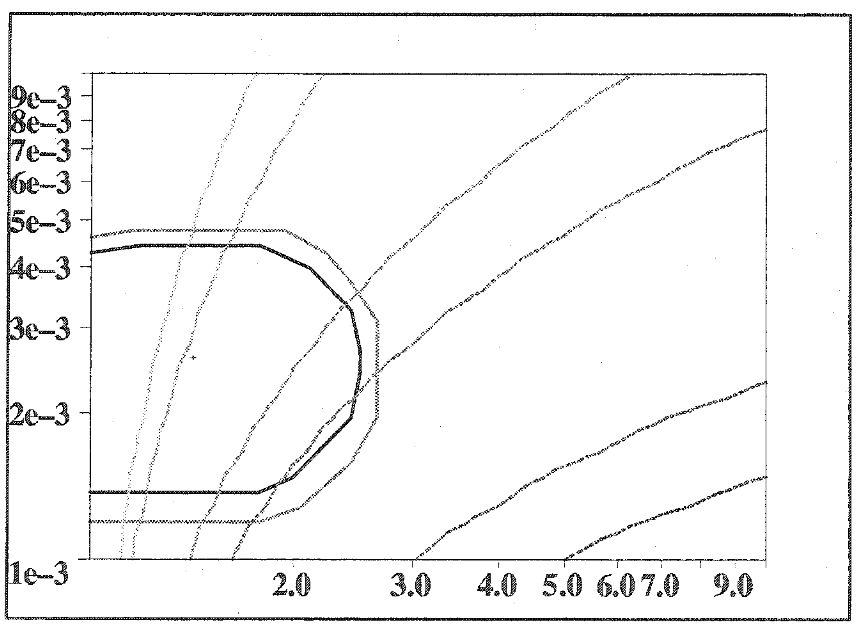

Figure 3.9: (LMA, +) contours (broken) of $(+t_3)^2$ =0.5, 1.0, 5.0, 10.0, 50.0, 100.0 $\times 10^{-6}$ for m_0 = 0.05eV, in the space of atmospheric parameters ($\Delta m_{32}^2/\mathrm{eV}^2$ against t_2^2) with the allowed region shown at 90 and 95%CL for $t_3^2 = 0.0$.

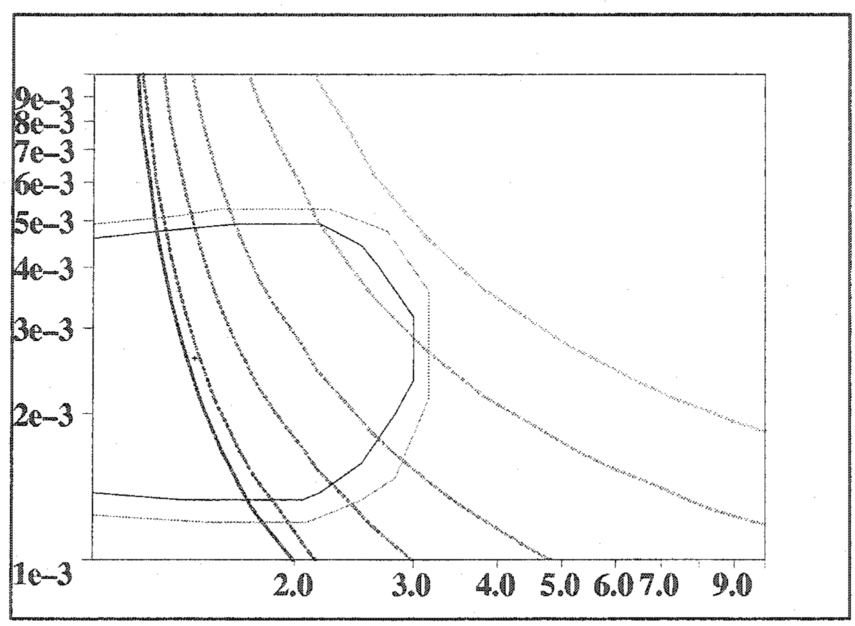

Figure 3.10: (LMA, $-$) contours of $(-t_3)^2$ =0.001, 0.002, 0.005, 0.01, 0.02 (broken) and 0.026 (solid) for m_0 = 0.05eV, in the space of atmospheric parameters ($\Delta m_{32}^2/\mathrm{eV}^2$ against t_2^2) with the allowed region shown at 90 and 95%CL for $t_3^2 = 0.01$.

Fig. 3.10 also shows contours of t_3^2, but these are calculated from the $t_3 < 0$ solution. The divergent behaviour along $t_2^2 = 1$ is clear as the CHOOZ boundary is exceeded for all small t_2^2.

These plots are representive: (LOW, $\pm$) will exhibit similar trends but will be characterised by much smaller t_3^2. Thus t_3^2 will be consistent with zero across most of the parameter space for all of the solutions except (LMA, $-$), for which the CHOOZ boundary is violated across a non-negligible region at small t_2^2. This will lead to difficulties in comparing (LMA, $-$) with the results of [26] which are presented in terms of planes of constant t_3^2. We will address these difficulties later.

Considering (LOW, $\pm$) and (LMA, $+$), for fixed m_0, the lower R bound excludes an area of large t_2^2 and large Δm_2^2. At lower values of m_0, the excluded area expands as in Fig. 3.11 and Fig. 3.12. Thus, the lower R bound is mobile (as m_0 varies) but the upper bound is essentially fixed very close to $t_2^2 = 1$. When the excluded area expands to include the best-fit (Fig. 3.12), which is marked by a cross, we have the minimum m_0 prediction. In essence, for larger values of m_0 there is better agreement between this model and experiment. As m_0 decreases more of the experimental region is excluded and the level of agreement worsens, until the situation becomes untenable when the best-fit point is excluded.

With this in mind we can claim that Fig. 3.11 represents a state of 95% agreement with experiment. Thus, we may state $0.01614 < m_0 \leq 0.0500$

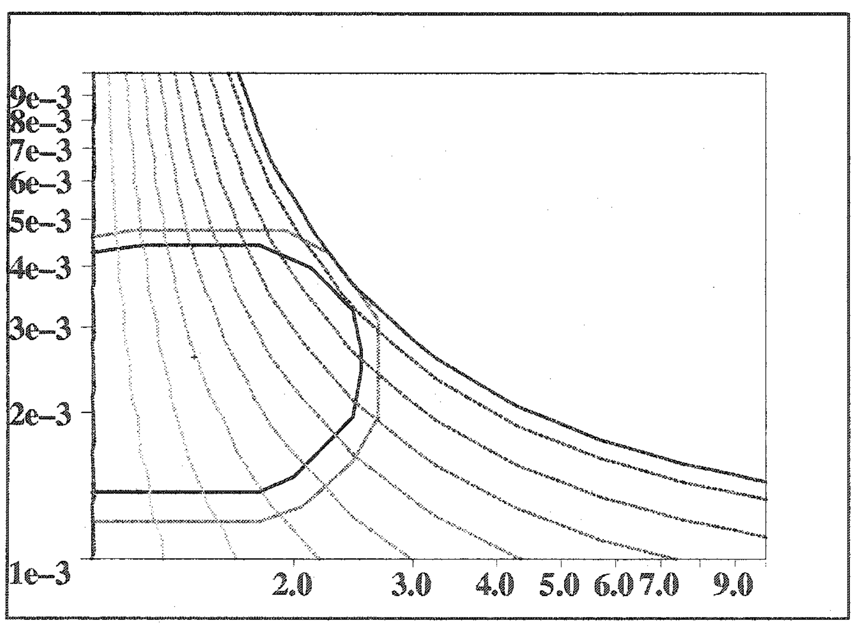

Figure 3.11: (LOW, $+$) contours of R =0.84, 0.86, 0.88, 0.90, 0.92, 0.94, 0.96, 0.98 (broken) and 0.8297, 0.99997 (solid) for $m_0 = 0.05$eV, in the space of atmospheric parameters ($\Delta m_{32}^2/\mathrm{eV}^2$ against t_2^2) with the allowed region shown at 90 and 95%CL for $t_3^2 = 0.0$.

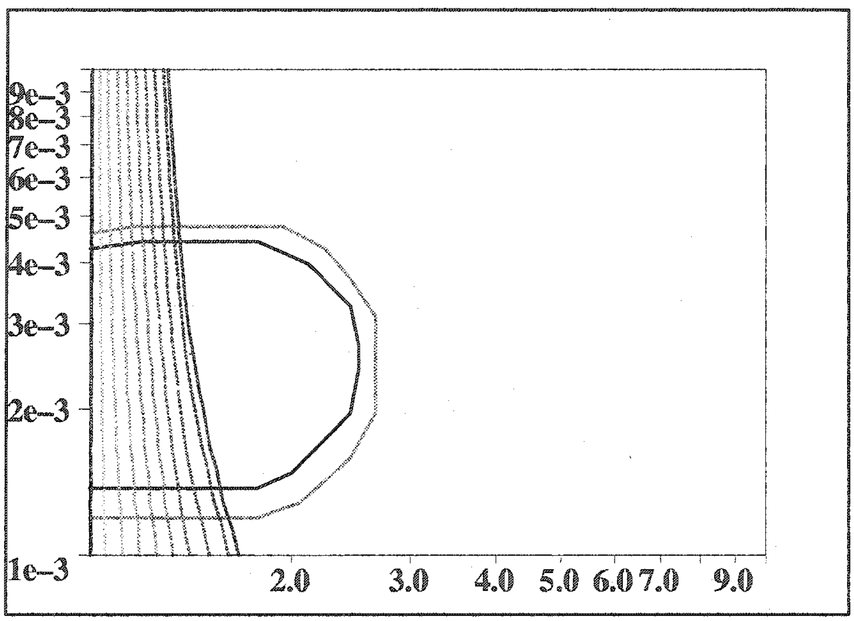

Figure 3.12: (LOW, +) contours of R =0.84, 0.86, 0.88, 0.90, 0.92, 0.94, 0.96, 0.98 (broken) and 0.8297, 0.99997 (solid) for m_0 = 0.01614eV, in the space of atmospheric parameters ($\Delta m^2_{32}/\mathrm{eV}^2$ against t^2_2) with the allowed region shown at 90 and 95%CL for t^2_3 = 0.0.

with 95% CL. Now, Fig. 3.11 and Fig. 3.12 are indicative of the behaviour of (LOW, $\pm$) and also of (LMA, $+$). So, in this way we may formulate prefered ranges for m_0 in each of these solutions, which are listed in Table 3.5.

Solution.	Range. (eV)	
	90% CL	95% CL
(LMA, $+$)	$0.01507 < m_0 \leq 0.0468$	$0.01507 < m_0 \leq 0.0499$
(LOW, $\pm$)	$0.01614 < m_0 \leq 0.0470$	$0.01614 < m_0 \leq 0.0500$

Table 3.5: Prefered ranges of m_0 for (LMA, $+$) and (LOW, $\pm$).

Note that these ranges are significantly more strict than those currently imposed by both tritium β-decay and $2\beta0\nu$ experiments.

The above behaviour in the atmospheric parameter space is for a fixed value of m_0, which leaves t_3 as a free parameter. This is reasonable for all of the solutions except (LMA, $-$) because t_3 remains small across the region of interest. But to compare (LMA, $-$) with experiment we must fix t_3.

For fixed t_3 the model becomes very sensitive to variation of the atmospheric parameters. This may be understood by recalling the asymptotic nature of t_3 at large m_0, and that when the input parameters are varied the asymptotic value will be altered.

Consider Fig. 3.13:

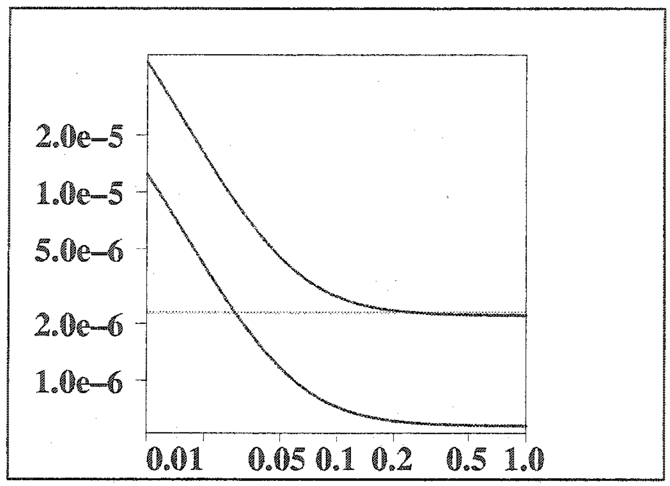

Figure 3.13: The asymptotic behaviour of t_3^2 against m_0: the lower curve is calculated at the best-fit, the upper curve is at $t_2^2 = 2.0$.

we choose a specific value of t_3 at which to examine the solutions of the model. If the inputs are varied in such a way that one of the solutions becomes asymptotic close to this value, we will see m_0 varying very rapidly, for even small changes in the asymptote: i.e. small changes in the input parameters. Indeed, it becomes impossible, at any reasonable resolution, to distinguish $m_0 \sim 0.2$eV from the direct-search bound of $m_0 = 2.2$eV (see Fig. 3.13).

Going a step further, it is apparent that certain values of the inputs, will not allow a solution for a given value of t_3^2: the asymptote of the solution will be greater than the chosen value of t_3^2 within a certain region of the parameter space.

Consequently, with fixed t_3^2 we find that (LMA, $-$) is insoluble within a region of the atmospheric parameter space, at the boundary of which m_0 diverges. The forbidden region is at small t_2^2 for all Δm_{32}^2. This is apparent in Fig. 3.14, where the close spacing of the left-most contours, namely 0.1 and 0.2eV, is indicative of the divergence close to them.

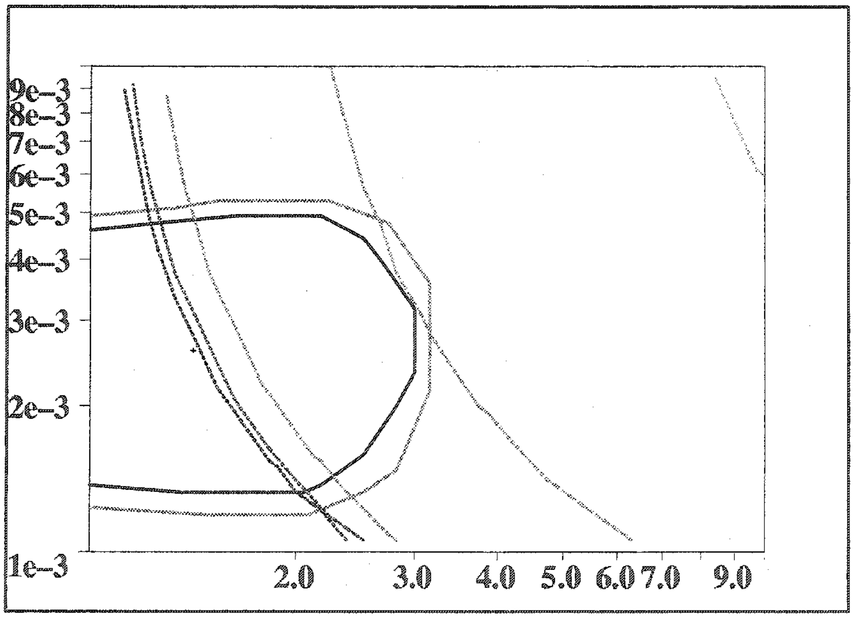

Figure 3.14: (LMA, $-$) contours of m_0 =0.005, 0.02, 0.05, 0.1 and 0.2eV for $(-t_3)^2 = 0.01$, in the space of atmospheric parameters ($\Delta m_{32}^2/\mathrm{eV}^2$ against t_2^2) with the allowed region shown at 90 and 95%CL for $t_3^2 = 0.01$.

Of special interest are the contours of R as seen in Fig. 3.15. $R = 0.9999$ coincides with the divergent boundary of m_0, as might be expected from the asymptotic behaviour of R at large m_0. The lower bound of R is quite nearby and in effect only a narrow band of the experimentally allowed region is in agreement with the requirements of the symmetry here.

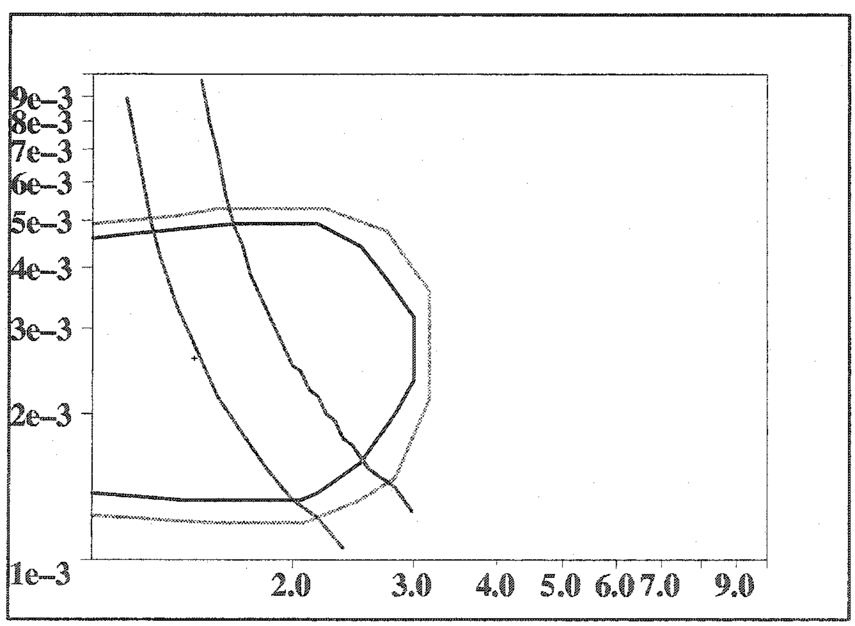

Figure 3.15: (LMA, $-$) contours of R =0.8297 (right) and 0.9999 (left) for $(-t_3)^2 = 0.01$, in the space of atmospheric parameters ($\Delta m^2_{32}/\mathrm{eV}^2$ against t_2^2) with the allowed region shown at 90 and 95%CL for $t_3^2 = 0.01$.

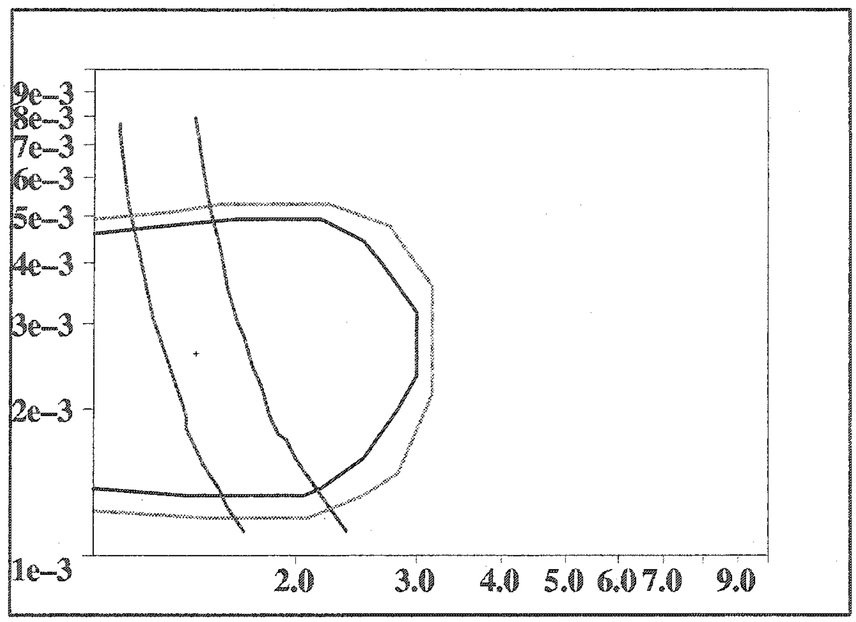

Figure 3.16: (LMA, $-$) contours of R =0.8297 (right) and 0.9999 (left) for $(-t_3)^2 = 0.026$, in the space of atmospheric parameters ($\Delta m^2_{32}/\mathrm{eV}^2$ against t_2^2) with the allowed region shown at 90 and 95%CL for $t_3^2 = 0.01$.

If t_3^2 is altered, the width of this band varies little and so there is no means of identifying a favoured set of parameters as was the case for (LOW, $\pm$) and (LMA, $+$). For example in Fig. 3.16 we see that the band between the R boundaries now contains the best-fit point (cross) and there may be marginally less overlap with the experimentally allowed region, compared to Fig. 3.15, but this is far from certain. We conclude that there are no particular limits on the (LMA, $-$) solution, using this means of analysis.

Conclusion.

A 2-3 exchange symmetry within the neutrino mass matrix, as it is defined at an energy scale appropriate to the See-saw mechanism and below which Supersymmetry is dominant, is consistent with current experimental data, as it is understood within the context of neutrino oscillations. The simple relationships of the exact 2-3 symmetry become quite complex under the influence of Renormalization Group running through the Supersymmetric regime. Through this process the parameters of the mixing matrix are interrelated, altering and distributing the effects of the original symmetry to include much of the matrix. In addition, the dynamics of the Renormalization Group Equations introduces new relationships and constraints. In this way, the possible range of $\tan\beta$ can restrict the size of a mass eigenvalue and the allowed range of the mass can then have its own effect upon the choice of $\tan\beta$.

Of particular interest is the robustness of the prediction of a minimum neutrino mass, first introduced in [29]. If the 2-3 symmetry is realised in nature and Supersymmetry does replace the Standard Model at higher energies, we have found that we can claim:

$$0.01614 < m_0 \lesssim 0.05 \tag{3.21}$$

with 95% Confidence Level. This statement is not only more stringent than current experimental bounds but also accessible to experiments planned for the near future [2].

By reflecting back the requirements upon m_0 and t_3^2 we have been able to comment upon the relevance of $\tan\beta$ in the context of this model. A general result is that $\tan\beta \gtrsim 13$, though this depends upon assumptions within the anaylsis of $2\beta 0\nu$. Additionally, for (LMA, $-$) alone there is a further constraint: $\tan\beta \lesssim 45$, which comes from the inherently large values of t_3^2 in this solution.

Other qualitative properties are equally important. The fact that this model distinguishes markedly between $\theta_3 > 0$ and $\theta_3 < 0$ or, equivalently, $\delta = 0$ and π gives us, at least in principle, a direct means of determining the Dirac phase in the neutrino mixing matrix.

Also, part of the LMA region in the solar parameter space is ruled out by the requirements of the symmetry in conjunction with the CHOOZ boundary, but the best-fit point remains within the allowed area.

Finally, perhaps the most interesting feature of this model is that it effectively halves the experimentally allowed region in the atmospheric parameter space. Furthermore, for the normal hierarchy, the symmetry prefers that part of the space containing the experimental best-fit and predicts the current condition of a very small but non-zero reactor angle. Experimentally, the symmetry of the atmospheric parameter space is itself broken by the non-vanishing reactor angle. For the 2-3 model the symmetry is broken by RG effects and a non-vanishing reactor angle is the result. It is intriguing that both broken symmetries should prefer the same region of parameter space and with the same criterion of non-zero θ_3.

Appendix A

Useful Identities for Dimensional Regularization [33].

Contraction and Trace Relations.

In D dimensions the set of $f(D) \times f(D)$ $(f(4) = 4)$ γ-matricies is: $\gamma^0, \gamma^1, \ldots, \gamma^{D-1}$. They satisfy:

$$\begin{aligned}
\gamma^\mu \gamma^\nu + \gamma^\nu \gamma^\mu &= 2g^{\mu\nu} \\
g_{\mu\nu} g^{\mu\nu} &= D \\
\gamma_\mu \gamma^\mu &= D\mathbb{I} \\
\gamma_\mu \gamma^\lambda \gamma^\mu &= -(D-2)\gamma^\lambda \\
\gamma_\mu \gamma^\sigma \gamma^\lambda \gamma^\mu &= (D-4)\gamma^\sigma \gamma^\lambda + 4g^{\sigma\lambda} \\
\mathrm{Tr}[\gamma^\sigma \gamma^\lambda] &= f(D) g^{\sigma\lambda} \\
\mathrm{Tr}[\gamma^\rho \gamma^\delta \gamma^\sigma \gamma^\lambda] &= f(D)[g^{\rho\delta} g^{\sigma\lambda} - g^{\rho\sigma} g^{\delta\lambda} + g^{\rho\lambda} g^{\delta\sigma}] \\
\mathrm{Tr}[\gamma^{\sigma_1} \gamma^{\sigma_2} \ldots \gamma^{\sigma(2m+1)})] &= 0, \text{ for any integer m.}
\end{aligned}$$

Standard Integrals.

After Feynman parameterisation we may use the following:

$$\begin{aligned}
\int \mathrm{d}^D k \frac{k^\mu}{(k^2+s)^n} &= 0 \\
\int \mathrm{d}^D k \frac{k^\mu k^\nu}{(k^2+s)^n} &= i\pi^{D/2} \frac{\Gamma(n-(D/2)-1)}{2\Gamma(n)} \frac{g^{\mu\nu}}{s^{n-(D/2)-1}} \\
\int \mathrm{d}^D k \frac{k^2}{(k^2+s)^n} &= i\pi^{D/2} \frac{\Gamma(n-(D/2)-1)}{2\Gamma(n)} \frac{D}{s^{n-(D/2)-1}}.
\end{aligned}$$

Bibliography

[1] F.Reines from the Preface of 'Spaceship Neutrino' (Cambridge University Press, Cambridge, 1992), by Christine Sutton, xiii.

[2] A. Osipowicz *et al.* (KATRIN Coll.), (2001) hep-ex/0109033.

[3] J. Bonn *et al.*, *Nucl. Phys. Proc. Suppl.* **91** (2001) 273.

[4] H. V. Klapdor-Kleingrothaus *et al.*, *Eur. Phys. J.* **A12** (2001) 147.

[5] H. V. Klapdor-Kleingrothaus *et al.*, (2002) hep-ph/0201231.

[6] F. Reines, C. L. Cowan, Jr., *Phys. Rev.* **92** (1953) 8301;
C. L. Cowan *et al.*, *Science* **124** (1956) 103.

[7] D. E. Groom *et al.* (Particle Data Group), *Eur. Phys. J.* **C15** (2000).

[8] B. Pontecorvo, *J. Exptl. Theoret. Phys.* **33** (1957) 549.

[9] G. Danby *et al.*, *Phys. Rev. Lett.* **9** (1962) 36.

[10] Z. Maki, M. Nakagawa and S. Sakata, *Prog. Theor. Phys.* **28** (1962) 870

[11] N. Cabibbo, *Phys. Rev. Lett.* **10** (1963) 531;
M. Kobayashi and K. Maskawa, *Prog. Theor. Phys.* **49** (1973) 652.

[12] L. Wolfenstein, *Phys. Rev. D* **17** (1978) 2369.

[13] S. P. Mikheyev and A. Yu Smirnov, *Yad. Fiz.* **42** (1985) 1441.

[14] R. Davis, Jr., D. S. Harmer and K. C. Hoffman, *Phys. Rev. Lett.* **20** (1968) 1205.

[15] J. N. Bahcall, H. M. Pinsonneault and S. Basu, *Astrophys. J.* **555** (2001) 990;
A. R. Junghans *et al.*, *Phys. Rev. Lett.* **88** (2002) 041101;
J. N. Bahcall, M. C. Gonzalez-Garcia and C. Peña-Garay, (2001) hep-ph/0111150.

[16] G. Fiorentini, B. Ricci and F. L. Villante, *Nucl. Phys. Proc. Suppl.* **95** (2001) 116;
J. Christensen-Dalsgaard, (2002) astro-ph/0207403.

[17] B. T. Cleveland *et al.*, *Astrophys. J.* **496** (1998) 505;
K. Lande *et al.*, *Nucl. Phys. Proc. Suppl.* **77** (1999) 13.

[18] V. N. Gavrin *et al.* (SAGE Coll.), *Nucl. Phys. Proc. Suppl.* **91** (2000) 36.

[19] W. Hampel *et al.* (GALLEX Coll.), *Phys. Lett. B* **447** (1999) 127.

[20] M. Altmann *et al.* (GNO Coll.), *Phys. Lett. B* **490** (2000) 16.

[21] Y. Fukuda *et al.* (Kamiokande Coll.), *Phys. Rev. Lett.* **77** (1996) 1683.

[22] S. Fukuda *et al.* (SuperKamiokande Coll.), *Phys. Rev. Lett.* **86** (2001) 5651.

[23] A. B. McDonald *et al.* (SNO Coll.), *Nucl. Phys. Proc. Suppl.* **91** (2000) 21.

[24] J. N. Bahcall, M. C. Gonzalez-Garcia and C. Peña-Garay, (2002) hep-ph/0204314.

[25] T. Toshito *et al.* (SuperKamiokande Coll.), (2001) hep-ex/0105023;
W. W. M. Allison *et al.* (Soudan Coll.), *Phys. Lett. B* **449** (1999) 137;
M. Ambrosio *et al.* (MACRO Coll.), *Phys. Lett. B* **517** (2001) 59.

[26] M. C. Gonzalez-Garcia and Y. Nir, (2002) hep-ph/0202058.

[27] S. M. Bilenky, J. Hosek and S. T. Petcov, *Phys. Lett. B* **94** (1980) 495; P. Langacker, S. T. Petcov, G. Steigman and S. Toshev, *Nucl. Phys. B* **282** (1987) 589.

[28] M. Apollonio *et al.* (CHOOZ Coll.), *Phys. Lett. B* **466** (1999) 415.

[29] C. S. Lam, *Phys. Lett. B* **507** (2001) 214.

[30] F. Halzen and A. D. Martin, *Quarks and Leptons*, John Wiley and Sons (1984) **0471887412**

[31] R. N. Mohapatra and G. Senjanović, *Phys. Rev. Lett.* **44** (1980) 912.

[32] E. Kh. Akhmedov, (2000) hep-ph/0001264.

[33] F. Mandl and G. Shaw, *Quantum Field Theory*, John Wiley and Sons (1993) **0471941867**

[34] T. P. Cheng, E. J. Eichten and L. F. Li, *Phys. Rev. D* **9** (1974) 2259.

[35] H. Murayama, (2000) hep-ph/0002232.

[36] B. Grzadkowski, M. Lindner and S. Theisen, *Phys. Lett. B* **198** (1987) 64.

[37] J. Ellis and S. Lola, (1999) hep-ph/9904279.

[38] M. C. Gonzalez-Garcia, M. Maltoni, C. Peña-Garay and J. W. F. Valle, *Phys. Rev. D* **63** (2001) 033005.